Numerical inverse scattering for the Korteweg–de Vries and modified Korteweg–de Vries equations

Thomas Trogdon,* Sheehan Olver† and Bernard Deconinck‡

1,3Department of Applied Mathematics
University of Washington
Campus Box 352420
Seattle, WA, 98195, USA

2Mathematical Institute
University of Oxford
24–29 St Giles'
Oxford, OX1 3LB, UK

August 15, 2011

Abstract

Recent advances in the numerical solution of Riemann–Hilbert problems allow for the implementation of a Cauchy initial value problem solver for the Korteweg–de Vries equation (KdV) and the defocusing modified Korteweg–de Vries equation (mKdV), without any boundary approximation. Borrowing ideas from the method of nonlinear steepest descent, this method is demonstrated to be asymptotically accurate. The method is straightforward for the case of defocusing mKdV due to the lack of poles in the Riemann–Hilbert problem and the boundedness properties of the reflection coefficient. Solving KdV requires the introduction of poles in the Riemann–Hilbert problem and more complicated deformations. The introduction of a new deformation for KdV allows for the stable asymptotic computation of the solution in the entire (x,t)-plane. KdV and mKdV are dispersive equations and this method can fully capture the dispersion with spectral accuracy. Thus, this method can be used as a benchmarking tool for determining the effectiveness of future numerical methods designed to capture dispersion. This method can easily be adapted to other integrable equations with Riemann–Hilbert formulations, such as the nonlinear Schrödinger equation.

1 Introduction

We consider the initial-value problem on the whole line for the Korteweg–de Vries equation (KdV)

$$q_t + 6qq_x + q_{xxx} = 0, \tag{1.1}$$
$$q(x,0) = q_0(x) \in \mathcal{S}(\mathbb{R}),$$

where subscripts denote partial differentiation and $\mathcal{S}(\mathbb{R})$ is the Schwartz class on $\mathbb{R}$ [1, Definition 4.2.1]. We also consider the defocusing modified Korteweg–de Vries equation (mKdV), given by

$$q_t - 6q^2 q_x + q_{xxx} = 0, \tag{1.2}$$
$$q(x,0) = q_0(x) \in \mathcal{S}(\mathbb{R}).$$

1email: trogdon@amath.washington.edu
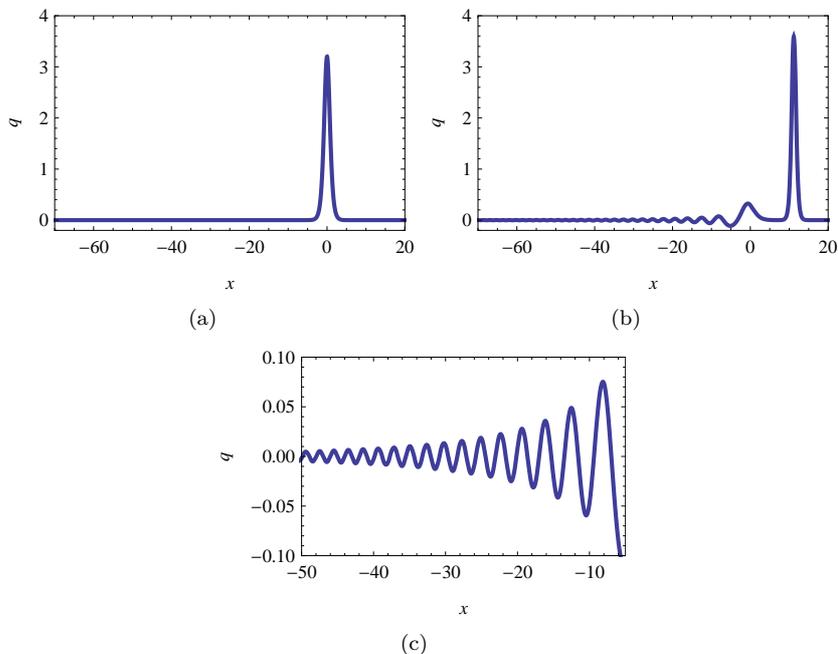2email: sheehan.olver@sjc.ox.ac.uk
3email: bernard@amath.washington.edu

Figure 1: Numerical solution of KdV with initial data that is close to a two-soliton solution. (a) Initial condition, (b) Solution at $t = 1.5$, (c) Dispersive tail at $t = 1.5$.

KdV describes the propagation of long waves in dispersive media, e.g. long surface water waves [2]. Historically, KdV is the first known case of a PDE that is solvable by the inverse scattering transform [3]. KdV and mKdV can also be thought of as dispersive regularizations of the Burgers and modified Burgers equations, respectively.

The presence of dispersion makes the approximation of solutions of KdV and mKdV through numerical methods especially difficult. The linear dispersion relation of KdV is cubic, which indicates that small waves travel with velocity proportional to the square of their wave numbers. A common method to solve the Cauchy problem on the line is to approximate it by a periodic solution over a large domain. Due to dispersion, non-trivial boundary contributions are present in the approximation early on. In Figure 1 we approximate the solution of KdV with $q(x, 0) = A \operatorname{sech}^2(x)$ where $A = 3.2$ using the numerical scheme presented here. With $A = 3$ the solution would be a two-soliton solution without any dispersive tail [4]. Notice that a significant dispersive tail forms even though the solution is close to the soliton case. The issue becomes worse when we consider solutions that are farther from a soliton solution, see Figure 2.

To combat this dispersive complication, we exploit the integrable structure of KdV and mKdV and evaluate the inverse scattering transform numerically. This involves developing techniques to compute the forward transform (direct scattering) and the inverse transform (inverse scattering). Our approach to direct scattering employs collocation methods and existing spectrum approximation techniques. For inverse scattering we use the numerical method for Riemann–Hilbert problems (RHPs) presented in [5]. After deforming the RHP in the spirit of Deift and Zhou [6, 7, 8] the numerical method becomes asymptotically accurate: the work required to compute the solution to a desired accuracy is bounded for all x and t. Note that in this method the role of x and t is reduced to that of parameters. No time-stepping or spatial discretization is needed.

We start off with background material concerning RHPs and their numerical solution. The numerical direct and inverse scattering for defocusing mKdV is then presented along with numerical results. The RHP for mKdV has a simple form and the deformations are straightforward. Next, KdV is considered. Now one has to deal with the addition of solitons to the problem. After deformation, the RHP for KdV has a singularity and this requires two additional deformations. We introduce a new deformation that is not
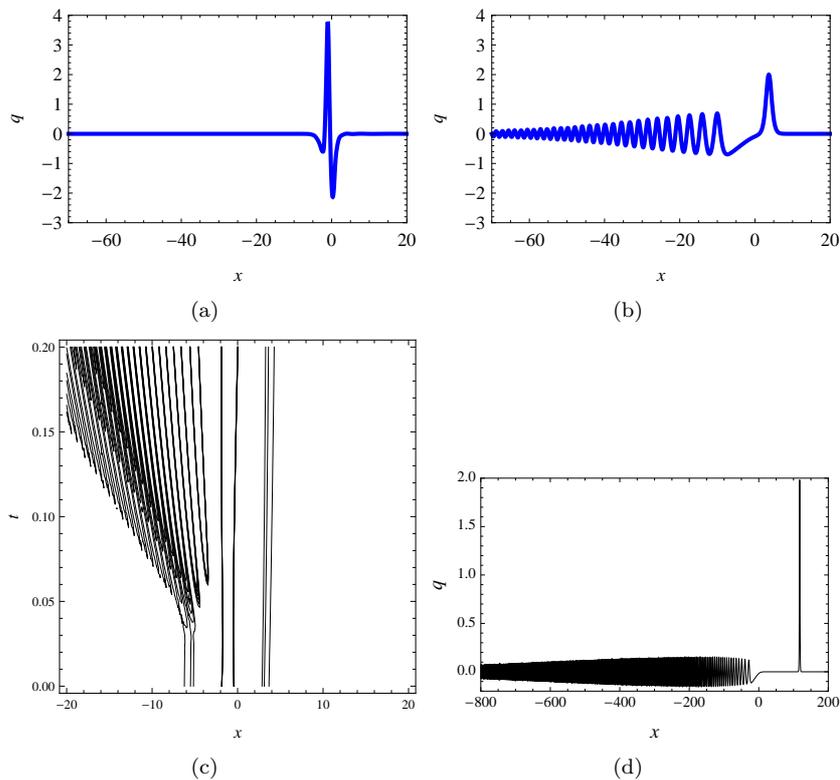
Figure 2: Numerical solution of KdV which is far from a pure soliton solution. (a) Initial condition obtained by adding a soliton to the RHP associated with $q(x, 0) = -2.3 \operatorname{sech}^2(x)$, (b) Solution at $t = 1.5$, (c) A contour plot showing the birth of the dispersive tail, (d) Solution at $t = 30$. Conventional spectral methods cannot capture this solution.

present, to our knowledge, in the existing literature. This new transition region allows for stable asymptotic computation of the solution in a region where the classical deformations break down numerically. Numerical results for KdV are presented. Finally, the numerical solutions of mKdV and KdV are compared using the Miura transformation.

We solve mKdV because the complexity associated with its solution is what should be expected when solving other integrable equations with this method. We solve KdV because it is a more difficult problem, and demonstrates that the method is general enough to handle the added difficulties, though it requires the introduction of significantly more machinery.

Through the comparison of our results with existing asymptotic expressions we can guarantee the accuracy of the method. It is accurate for small-time as well as long-time. Traditionally, numerical analysts have favored integrable equations because of the large class of explicit solutions available for comparison. All of these explicit cases do not exhibit a dispersive tail. This method expands the class of solutions which we can compute accurately and, importantly, it provides a benchmark test to guide the development of new numerical methods designed to capture dispersion.

2 Background Material

We use this section to introduce a few fundamental results and fix notation. A reader looking for a more in-depth discussion of RHPs should look to [9] for a introduction and [10, 11, 12] for a more advanced discussion. A good reference for the solution of differential equations with collocation methods is [1]. A comprehensive discussion of the inverse scattering transform can be found in [13, 14].
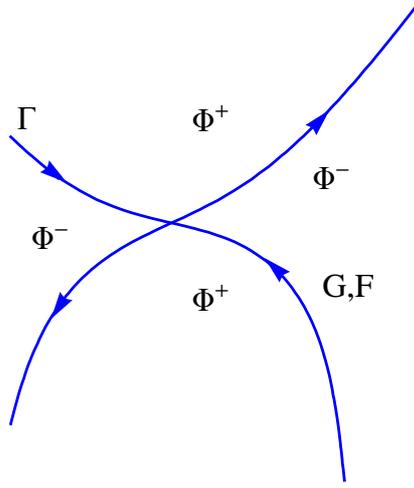
3

Figure 3: An example contour in the complex k-plane with self-intersections.

2.1 Cauchy Operators and Riemann–Hilbert Problems

Given a closed, oriented contour Γ and functions $G : \Gamma \to \mathbb{C}^{j \times j}$, $F : \Gamma \to \mathbb{C}^{i \times j}$, a RHP poses the task of finding a function $\Phi : \Gamma \to \mathbb{C}^{i \times j}$, analytic in $\mathbb{C} \setminus \Gamma$ and continuous up to Γ so that

$$\Phi^+(k) = \Phi^-(k)G(k) + F(k), \quad k \in \Gamma, \tag{2.1}$$

$$\Phi(\infty) = \Phi_\infty, \tag{2.2}$$

where Φ_∞ is a constant matrix. Let Φ^+ and Φ^- denote the representation of Φ in different regions of the complex k-plane, see Figure 3. In (2.1), Φ^+ and Φ^- denote the limit values of Φ when the limit is taken in the appropriate regions. We also use $\Phi_\pm$ to denote the same limits when this makes notation more concise.

Define the Cauchy integral (applied componentwise) by

$$\mathcal{C}_\Gamma f(k) = \frac{1}{2\pi i} \int_\Gamma \frac{f(t)}{t - k} dt, \text{ for } k \notin \Gamma.$$

This defines an analytic function for $k \notin \Gamma$. Let Γ_0 be the set of self-intersection points of Γ. We define the Cauchy transform pair by

$$\mathcal{C}_\Gamma^\pm f(k) = \lim_{\epsilon \to 0^\pm} \frac{1}{2\pi i} \int_\Gamma \frac{f(t)}{t - (k \pm \eta \epsilon)} dt, \text{ for } k \in \Gamma \setminus \Gamma_0,$$

where η is the positive unit normal. The so-called Plemelj formulae hold [9],

$$\begin{aligned} \mathcal{C}_\Gamma^+ f(k) - \mathcal{C}_\Gamma^- f(k) &= f(k), \quad k \in \Gamma \setminus \Gamma_0, \\ \mathcal{C}_\Gamma^+ f(k) + \mathcal{C}_\Gamma^- f(k) &= -i\mathcal{H}_\Gamma f(k), \quad k \in \Gamma \setminus \Gamma_0, \end{aligned} \tag{2.3}$$

where $\mathcal{H}_\Gamma$ is the Hilbert transform defined by the principal-value integral

$$\mathcal{H}_\Gamma f(k) = \lim_{\epsilon \to 0} \frac{1}{\pi} \int_{\Gamma_\epsilon(k)} \frac{f(t)}{t - k} dt, \quad \Gamma_\epsilon(k) = \{t \in \Gamma : |k - t| \geq \epsilon\}.$$

Remark 2.1. The sense in which the above limits exist depends on the regularity of f [10].

Definition 2.1. If $\Gamma_n \subset \Gamma$ is also a contour and $f : \Gamma \to \mathbb{C}$, we define $f|_{\Gamma_n}$ to be the restriction of f to Γ_n.

Definition 2.2. Assume that $a \in \Gamma_0$ and let $\Gamma_1, \ldots, \Gamma_n$ be a counter-clockwise ordering of subcomponents which contain $k = a$ as an endpoint. Let

$$\hat{G}_i = \begin{cases} (G|_{\Gamma_i})^{-1} & \text{if } \Gamma_i \text{ is oriented outward,} \\ G|_{\Gamma_i} & \text{if } \Gamma_i \text{ is oriented inward.} \end{cases}$$

We say that the RHP satisfies the product condition if

$$\prod_{i=1}^{n} \hat{G}_i(a) = I,$$

for every $a \in \Gamma_0$.

The class of RHPs we consider have solutions of the form

$$\Phi(k) = \frac{1}{2\pi i} \int_\Gamma \frac{u(t)}{t-k} dt + \Phi_\infty \tag{2.4}$$

for some function u [15]. This relationship is the basis for a large number of explicit solution techniques and it is used directly in the numerical method presented below.

2.2 A Numerical Method for Riemann–Hilbert Problems

Consider the contour $\Gamma = \bigcup_{j=1}^{n} \Gamma_j$ where each Γ_j is a non-self-intersecting arc. Also, we assume we have a sequence of Möbius transformations $M_1, \ldots, M_n$ such that $M_k([-1,1]) = \Gamma_k$. Define $\mathbb{P}_m = \{\cos(j\pi/m) : j = 0, 1, \ldots, m\}$, the Chebyshev points, and let $T_m(x)$ denote the mth Chebyshev polynomial of the first kind. Given a RHP which satisfies the product condition on Γ, the framework in [5] will generally return a vector V_j of values at the mapped points $M_j(\mathbb{P}_{n_j})$, so that the function $U : \Gamma \to \mathbb{C}^{i \times j}$ defined piecewise by

$$U(k)|_{\Gamma_j} = \sum_{i=0}^{n_j} \alpha_i T_i(M_j^{-1}(k)),$$

$$U(M(\mathbb{P}_{n_j})) = V_j,$$

satisfies

- $I + \mathcal{C}_\Gamma U$ is bounded,

- $I + \mathcal{C}_\Gamma U$ satisfies the RHP exactly at $M_j(\mathbb{P}_{n_j})$,

where I denotes the identity matrix. If $\Phi_\infty = 0$ we use (2.4) and note that if $u \in L^1(\Gamma)$ then

$$\lim_{k \to \infty} k\Phi(k) = -\frac{1}{2\pi i} \int_\Gamma u(t)dt,$$

by dominated convergence. The integral on the right-hand side can be computed using Clenshaw–Curtis quadrature. This relationship is needed in what follows to reconstruct the solution to KdV or mKdV from the solution of the RHP. The framework in [16, 5] gives an efficient method for computing $\mathcal{C}_\Gamma$.

Remark 2.2. From the results in [5] it follows that convergence can be verified *a posteriori* by checking that the norm of the inverse of a collocation matrix grows at most algebraically. In the computations for this paper, we noticed at most logarithmic growth of the condition number for this collocation matrix, with a maximum on the order of 10^3.

2.3 Integrability and Lax Pairs

MKdV and KdV and are both completely integrable [13]. We take this to mean that for each equation there exist two linear systems of ordinary differential equations depending on a parameter k

$$\mu_x = L(k, q)\mu,$$
$$\mu_t = M(k, q)\mu,$$

such that $\mu_{xt} = \mu_{tx}$ if and only if q satisfies the PDE in question. Systems of this form are called Lax pairs. They are referred to sometimes as the scattering problem for the PDE. We introduce the modified Zakharov–Shabat scattering problem given by

$$\mu_x = \begin{pmatrix} -ik & q \\ r & ik \end{pmatrix} \mu,$$
$$\mu_t = \begin{pmatrix} A & B \\ C & D \end{pmatrix} \mu,$$

where q, r, A, B, C and D are scalar functions to be determined [13]. If we make the choice

$$
\begin{aligned}
A &= -4ik^3 + 2ikqr - (r_x q - q_x r), \\
B &= 4qk^2 + 2ikq_x - 2q^2 r - q_{xx}, \\
C &= 4rk^2 - 2ikr_x + 2qr^2 - r_{xx}, \\
D &= -A,
\end{aligned}
\tag{2.5}
$$

we can obtain Lax pairs for both mKdV and KdV.

2.3.1 The Modified Korteweg–de Vries Equation

To obtain a Lax pair for (defocusing) mKdV (1.2), let $r = q$, so that the x equation of the Lax pair takes the form

$$\mu_x = \begin{pmatrix} -ik & q \\ q & ik \end{pmatrix} \mu. \tag{2.6}$$

In what follows we do not need the explicit form of the equation for μ_t.

Remark 2.3. We perform scattering in a more restricted space of functions. Define, for $\delta > 0$,

$$\mathcal{S}_\delta(\mathbb{R}) = \{f \in \mathcal{S}(\mathbb{R}) : \lim_{|x| \to \infty} |f| e^{\delta |x|} = 0\}.$$

Assuming that $q(x, 0) \in \mathcal{S}_\delta(\mathbb{R})$ simplifies some technical details as is noted below. This assumption can be relaxed on a case-by-case basis. The decay rate is needed for analyticity properties and the smoothness is needed to numerically compute the scattering data, defined below.

1. *Definition of the Scattering Data.* Consider the problem (2.6). Assume $q \in \mathcal{S}_\delta(\mathbb{R})$, it follows that there are two matrix valued eigenfunctions

$$\phi(x; k) \backsim \begin{pmatrix} e^{-ikx} & 0 \\ 0 & -e^{ikx} \end{pmatrix} \text{ as } x \to -\infty, \quad \psi(x; k) \backsim \begin{pmatrix} e^{-ikx} & 0 \\ 0 & e^{ikx} \end{pmatrix} \text{ as } x \to \infty. \tag{2.7}$$

From Abel's formula, the determinants of these solutions are constant in x; evaluating at $\pm\infty$ we see that the columns do indeed form a linearly independent solution set and hence span the solution space. There exists a transition matrix

$$T(k) = \begin{pmatrix} a(k) & \mathcal{B}(k) \\ b(k) & \mathcal{A}(k) \end{pmatrix},$$

such that

$$\phi(x; k) = \psi(x; k)T(k).$$

Define $\rho(k) = b(k)/a(k)$ to be the reflection coefficient. For defocusing mKdV we define the scattering data to be only the reflection coefficient [13]. The conventions for the reflection coefficient in [13] and [6] differ. The reflection coefficient used by Ablowitz and Segur [13] is i times that used by Deift and Zhou [6].

2. *The Inverse Problem.* We phrase the inverse problem in terms of a RHP. We seek a sectionally analytic 2×2 matrix-valued function Φ that satisfies

$$\Phi^+(k; x, t) = \Phi^-(k; x, t)G(k; x, t), \quad k \in \mathbb{R},$$
$$\Phi(\infty; x, t) = I,$$
$$G(k; x, t) = \begin{pmatrix} 1 - \rho(k)\rho(-k) & -\rho(-k)e^{-\theta(k)} \\ \rho(k)e^{\theta(k)} & 1 \end{pmatrix},$$
$$\theta(k) = 2ikx + 8ik^3t.$$

The solution to mKdV is given by

$$q(x, t) = -2i \lim_{k \to \infty} k\Phi(k; x, t)_{21}, \tag{2.8}$$

where the subscript denotes the 2-1 component [6].

Remark 2.4. The well-posedness of this RHP can be established by considering a specific singular integral equation and showing it is of the form $(I - K)u = f$ where $\|K\| < 1$. This fact relies on $\sup_{k \in \mathbb{R}} |\rho(k)| < 1$, see [6] for details.

2.3.2 The Korteweg–de Vries Equation

To obtain KdV (1.1) from (2.5) we set $r = -1$ and the x portion of Lax pair takes the form

$$\mu_x = \begin{pmatrix} -ik & q \\ -1 & ik \end{pmatrix} \mu.$$

This can be further reduced to the time-independent Schrödinger equation

$$\mu_{xx} + (k^2 - q)\mu = 0. \tag{2.9}$$

As before, we do not need the explicit form of the equation for μ_t.

1. *Definition of the Scattering Data.* We consider the problem (2.9) and assume $q \in \mathcal{S}_\delta(\mathbb{R})$. There are two vector-valued eigenfunctions

$$\phi \frown \begin{pmatrix} e^{-ikx} & e^{ikx} \end{pmatrix} \text{ as } x \to -\infty, \quad \psi \frown \begin{pmatrix} e^{-ikx} & e^{ikx} \end{pmatrix} \text{ as } x \to \infty.$$

It follows from Abel's formula that the Wronskian of these solutions is constant in x and evaluating at $\pm\infty$ we see the two entries form a linearly independent solution set which spans the solution space. There is a transition matrix

$$T(k) = \begin{pmatrix} a(k) & b(k) \\ \mathcal{B}(k) & \mathcal{A}(k) \end{pmatrix},$$

such that $\phi(x, t; k) = \psi(x, t; k)T(k)$. Define $\rho(k) = b(k)/a(k)$ to be the reflection coefficient. It is known that $a(k)$ has simple zeros in the upper-half plane, on the imaginary axis. We denote the set of these n zeros by $\{\kappa_j\}_{j=1}^n$ and we assume that $\rho(k)$ can be analytically extended above these poles. In this case let $C_j = \text{Res}\{\rho(k), k = \kappa_j\}$ and form the set $\{C_j\}_{j=1}^n$. Define the set

$$\{\rho(k), \{\kappa_j\}_{j=1}^n, \{C_j\}_{j=1}^n\}, \tag{2.10}$$

to be the scattering data for KdV.

2. *The Inverse Problem.* We can pose the meromorphic RHP for the solution of KdV. We seek a function $\Phi : \mathbb{R} \to \mathbb{C}^{1 \times 2}$ that is meromorphic off $\mathbb{R}$ with simple poles at $\pm \kappa_j$ such that

$$\Phi^+(k; x, t) = \Phi^-(k; x, t) G(k; x, t), \quad k \in \mathbb{R},$$

$$\mathrm{Res}\{\Phi(k; x, t), k = \kappa_j\} = \lim_{k \to \kappa_j} \begin{pmatrix} 0 & 0 \\ C_j e^{\theta(\kappa_j)} & 0 \end{pmatrix} \Phi(k; x, t),$$

$$\mathrm{Res}\{\Phi(k; x, t), k = -\kappa_j\} = \lim_{k \to -\kappa_j} \begin{pmatrix} 0 & -C_j e^{\theta(\kappa_j)} \\ 0 & 0 \end{pmatrix} \Phi(k; x, t),$$

$$\Phi(\infty; x, t) = \begin{pmatrix} 1 & 1 \end{pmatrix}.$$

The solution to KdV is given by the reconstruction formula [14],

$$q(x, t) = 2i \lim_{k \to \infty} k \Phi_x(k; x, t)_1.$$

Remark 2.5. Due to the fact that generically $\rho(0) = -1$ for KdV the well-posedness of this RHP is more difficult to establish, see [8].

Remark 2.6. This meromorphic problem can be turned into an analytic problem by introducing small circles around each pole and using the appropriate jump on this new contour [8]. Fix $0 < \epsilon < \min_{k \neq j} |\kappa_j - \kappa_k|/2$, with $\epsilon < \min_j |\kappa_j|$. This ϵ is chosen so that the circles $A_j^\pm = \{k \in \mathbb{C} : |k - \pm\kappa_j| < \epsilon\}$ do not intersect each other or the real axis. We define $\hat{\Phi}$ by

$$\hat{\Phi}(k; x, t) = \begin{cases} \Phi(k; x, t) \begin{pmatrix} 1 & 0 \\ -C_j e^{\theta(\kappa_j)}/(k - \kappa_j) & 1 \end{pmatrix}, & \text{if } |k - \kappa_j| < \epsilon, \ j = 1, \dots, n, \\[2ex] \Phi(k; x, t) \begin{pmatrix} 1 & 0 \\ C_j e^{\theta(\kappa_j)}/(k + \kappa_j) & 1 \end{pmatrix}, & \text{if } |k + \kappa_j| < \epsilon, \ j = 1, \dots, n, \\[2ex] \Phi(k; x, t), & \text{otherwise.} \end{cases}$$

It is straightforward to show that $\hat{\Phi}$ solves the RHP:

$$\hat{\Phi}^+(k; x, t) = \begin{cases} \hat{\Phi}^-(k; x, t) G(k; x, t), & \text{if } k \in \mathbb{R}, \\[2ex] \hat{\Phi}^-(k; x, t) \begin{pmatrix} 1 & 0 \\ -C_j e^{\theta(\kappa_j)}/(k - \kappa_j) & 1 \end{pmatrix}, & \text{if } k \in A_j^+, \\[2ex] \hat{\Phi}^-(k; x, t) \begin{pmatrix} 1 & -C_j e^{\theta(\kappa_j)}/(k + \kappa_j) \\ 0 & 1 \end{pmatrix}, & \text{if } k \in A_j^-, \end{cases}$$

$$\hat{\Phi}(\infty; x, t) = \begin{pmatrix} 1 & 1 \end{pmatrix},$$

where $A_j^- (A_j^+)$ has (counter-)clockwise orientation.

2.4 Asymptotic Regions

In this section we present the classical results on the long-time asymptotics of the solution of mKdV and KdV. We introduce constants, c_i, to divide regions. While any valid choice of these will work, the numerical method can be improved by adjusting these on a case-by-case basis.
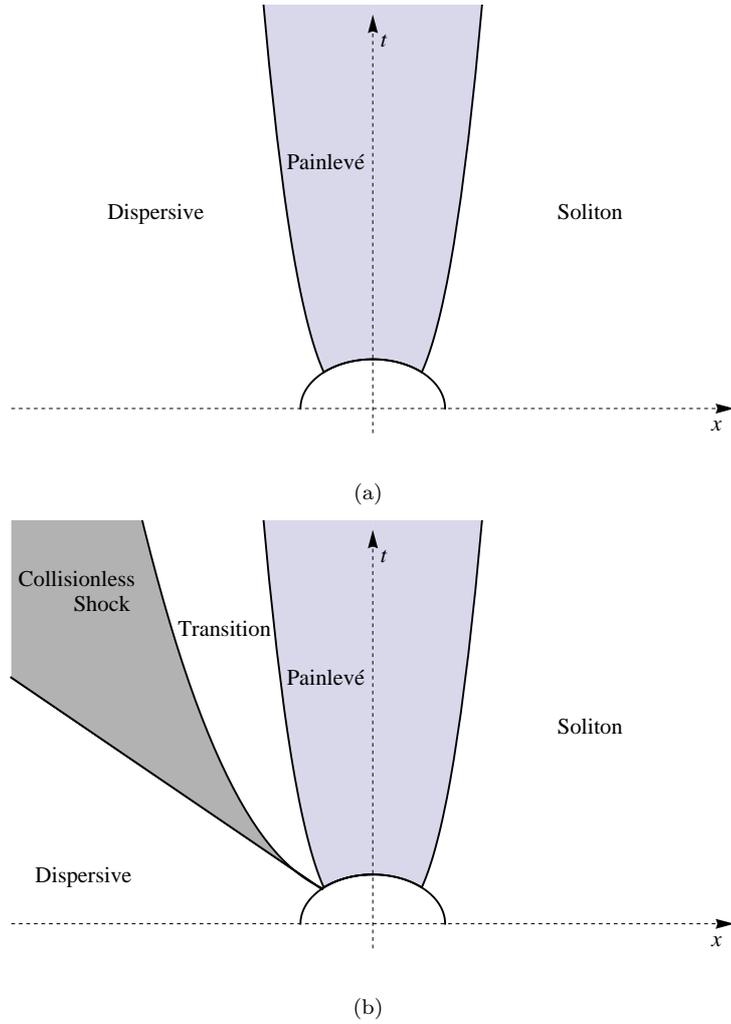
Figure 4: (a) Regions for the asymptotic analysis for mKdV, (b) Regions for the asymptotic analysis for KdV.

2.4.1 The Modified Korteweg–de Vries Equation

The results presented here are found in [6]. In the (x, t)-plane, the long-time evolution of mKdV is described in three fundamentally different ways. For a diagram of these regions see Figure 4(a).

1. *The Soliton Region.* This region is defined for $x \geq c_1 t^{1/3}$, $c_1 > 0$. The name "soliton region" is a misnomer because there are no solitons present in defocusing mKdV [13] but for the sake of uniformity with KdV we retain the name. Here the solution $q(x, t)$ decays beyond all orders, i.e.,

$$q(x, t) = \mathcal{O}((x + t)^{-j}), \quad \text{for all } j > 0. \tag{2.11}$$

2. *The Painlevé Region.* This region is defined for $|x| \leq c_1 t^{1/3}$. More general results can be found in [6]. Along a trajectory $x = -Ct^{1/3}$, $C > 0$, the solution satisfies

$$q(x, t) - U(x, t) = \mathcal{O}(t^{-2/3}), \tag{2.12}$$

where

$$U(x, t) = (3t)^{-1/3} v(x/(3t)^{1/3}), \tag{2.13}$$

9

and v is the Ablowitz–Segur solution to Painlevé II with Stokes constants $\{s_1, s_2, s_3\} = \{-i\rho(0), 0, i\rho(0)\}$.

3. *The Dispersive Region.* Historically, this region is defined for $-x > c_2 t > 0$, $c_2 > 0$. For our purposes, we use $-x > c_1 t^{1/3}$ for the definition of this region. The reasoning for this will become clear below. Along a trajectory $-x = Ct$, $C > 0$, the solution satisfies

$$q(x,t) - R(x,t) = \mathcal{O}(log(t)t^{-1}), \tag{2.14}$$

where

$$R(x,t) = \sqrt{\frac{\nu(k_0)}{3tk_0}} \cos\left(16tk_0^3 - \nu(k_0)\log(192tk_0^3) + \delta(k_0)\right),$$

and

$$k_0 = \sqrt{-x/(12t)},$$
$$\nu(k_0) = -\frac{1}{2\pi}\log(1 - \rho(k_0)\overline{\rho}(k_0)),$$
$$\delta(k_0) = \frac{\pi}{4} - \arg(\rho(k_0)) + \arg(\Gamma(i\nu(k_0)))$$
$$- \frac{1}{\pi}\int_{-k_0}^{k_0} \log\left(\frac{1 - \rho(\eta)\overline{\rho}(\eta)}{1 - \rho(k_0)\overline{\rho}(k_0)}\right)\frac{1}{\eta - k_0}d\eta.$$

2.4.2 The Korteweg–de Vries Equation

The results presented here are found in [7, 8]. See Figure 4(b) for a diagram of these regions.

1. *The Soliton Region.* This region is defined for $x \geq c_1 t^{1/3}$, $c_1 > 0$. For $x > Ct$, $C > 0$, the solution of KdV in this region satisfies

$$q(x,t) - S(x,t) = \mathcal{O}((x + t)^{-j}),$$

where

$$S(x,t) = 2\sum_{j=1}^{n} \kappa_j^2 \operatorname{sech}^2(\kappa_j x - 4\kappa_j^3 t - p_j),$$

$$p_j = \frac{1}{2}\log\left(\frac{C_j^2}{2\kappa_j}\prod_{l=j+1}^{n}\left(\frac{\kappa_l - \kappa_j}{\kappa_l + \kappa_j}\right)^2\right).$$

The constants κ_j and C_j are defined in (2.10).

2. *The Painlevé Region.* This region is defined for $|x| < c_1 t^{1/3}$. Along a trajectory $x = \pm Ct^{1/3}$, $C > 0$, the solution to KdV satisfies

$$q(x,t) - U(x,t) = \mathcal{O}(t^{-1}), \tag{2.15}$$

where

$$U(x,t) = \frac{1}{(3t)^{2/3}}\left(v^2\left(\frac{x}{(3t)^{1/3}}\right) + v'\left(\frac{x}{(3t)^{1/3}}\right)\right),$$

and v is the Hastings–McLeod solution to Painlevé II with Stokes constants $\{s_1, s_2, s_3\} = \{i, 0, -i\}$ [17]. The error bound is not present in [7] but we infer it from (2.12) through the Miura transformation §4.4.

3. *Transition Region.* This region is, to our knowledge, not present in the literature. It is defined by the relation $c_2 t^{1/3}(\log t)^{2/3} \leq -x \leq c_1 t^{1/3}$, $c_2 > 0$. Asymptotics are not known in this region.

10

4. *The Collisionless Shock Region.* This region is defined by $c_3 t \le -x \le c_2 t^{1/3}(\log t)^{2/3}$, $0 < c_3 \le 12$. This is the region in the (x, t)-plane where our deformations are valid. The asymptotic formula in [7] is given with the constraint $1/C \le -x/(t^{1/3}(\log t)^{2/3}) \le C$ for $C > 1$. With this constraint the RHP limits to a RHP on $(-b(s), b(s))$ of the form [7]

$$\zeta^+(k; x, t) = \begin{cases} \zeta^-(k; x, t) \begin{pmatrix} 0 & e^{-24i\tau \int_0^{a(s)} f(p)dp} \\ -e^{24i\tau \int_0^{a(s)} f(p)dp} & 0 \end{pmatrix}, & \text{if } a(s) < k < b(s), \\[2em] \zeta^-(k; x, t) \begin{pmatrix} 2\nu k^2 & 0 \\ 0 & (2\nu k^2)^{-1} \end{pmatrix}, & \text{if } -a(s) < k < a(s), \\[2em] \zeta^-(k; x, t) \begin{pmatrix} 0 & e^{-24i\tau \int_0^{-a(s)} f(p)dp} \\ -e^{24i\tau \int_0^{-a(s)} f(p)dp} & 0 \end{pmatrix}, & \text{if } -b(s) < k < -a(s), \end{cases}$$

$$\zeta(\infty) = \begin{pmatrix} 1 & 1 \end{pmatrix},$$
$$f(p) = \sqrt{(a^2 - p^2)(b^2 - p^2)}.$$

$$(2.16)$$

The definitions of a, b, s and τ can be found in Appendix C. See §4.2.3 for the definition of ν. Note that the only x and t dependence enters through a, b and τ. The approximation W of KdV is obtained by

$$W(x, t) = 2i\sqrt{-x/(12t)} \lim_{k \to \infty} \partial_x \zeta(k; x, t).$$

5. *The Dispersive Region.* This region is defined by $-x > c_3 t > 0$. Along a trajectory $x = -Ct$, $C > 0$, the solution to KdV satisfies

$$q(x, t) - R(x, t) = \mathcal{O}(t^{-1}), \tag{2.17}$$

where

$$R(x, t) = -\sqrt{\frac{4\nu(k_0)k_0}{3t}} \sin\left(16tk_0^3 - \nu(k_0)\log(192tk_0^3) + \delta(k_0)\right),$$

and

$$k_0 = \sqrt{-x/(12t)},$$
$$\nu(k_0) = -\frac{1}{2\pi} \log(1 - \rho(k_0)\overline{\rho}(k_0)),$$
$$\delta(k_0) = \frac{\pi}{4} - \arg(\rho(k_0)) + \arg(\Gamma(i\nu(k_0))) + \sum_{j=1}^{n} \arctan\left(\frac{\kappa_j}{k_0}\right)$$
$$- \frac{1}{\pi} \int_{-k_0}^{k_0} \log\left(\frac{1 - \rho(\eta)\overline{\rho}(\eta)}{1 - \rho(k_0)\overline{\rho}(k_0)}\right) \frac{1}{\eta - k_0} d\eta.$$

3 The Modified Korteweg–de Vries Equation

3.1 Numerical Computation of the Scattering Data

We look for solutions of the form (2.7) to (2.6). Define

$$\sigma_3 = \begin{pmatrix} 1 & 0 \\ 0 & -1 \end{pmatrix}, \quad \sigma_1 = \begin{pmatrix} 0 & 1 \\ 1 & 0 \end{pmatrix},$$

and two new functions

$$J(k; x, t) = \phi(k; x, t)\sigma_3 e^{ikx\sigma_3} - I,$$
$$K(k; x, t) = \psi(k; x, t)e^{ikx\sigma_3} - I. \tag{3.1}$$

Therefore $J \to 0$ as $x \to -\infty$ and $K \to 0$ as $x \to \infty$. Rewriting (2.7),

$$\mu_x = q\sigma_1\mu - ik\sigma_3\mu,$$

and we find that K and J both solve

$$M_x - ik[M, \sigma_3] - q\sigma_1 M = q\sigma_1,$$

For each k, this can be solved with a Chebyshev collocation method on $(-\infty, 0]$ for J and on $[0, \infty)$ for K using the appropriate boundary condition at infinity. (We conformally map the unbounded domains to the unit interval using $(1 + x)/(1 - x)$ and $(x - 1)/(1 + x)$.) If we use n collocation points, this gives two approximate solutions J_n and K_n for J and K, respectively. From J_n and K_n we obtain ϕ_n and ψ_n, approximations of ϕ and ψ, respectively, by inverting (3.1). Furthermore, ϕ_n and ψ_n share the point $x = 0$ in their domain of definition. Define

$$T_n(k) = \psi_n^{-1}(0; k)\phi_n(0; k).$$

This is an approximation of the transition matrix, from which we extract an approximation of the reflection coefficient.

3.2 Numerical Solution of the Inverse Problem

The RHPs considered here have the key feature that the jump matrices are highly oscillatory. Deift and Zhou adapted ideas from the asymptotic evaluation of integrals to this problem to obtain asymptotic formulae with rigorous error bounds [6, 10, 7]. The main idea of this method is to deform the contours of the RHP so that it limits (in some sense) to a simple problem that can be solved explicitly. In general, these same ideas translate to the numerics. The exponential decay that is sought in the analytic method also enables the fast convergence of the numerical approximation, as the smoothness of the resulting asymptotic expansions ensure that the solution to the RHP can be well represented by mapped Chebyshev polynomials. In what follows we deform the RHP for mKdV. The deformations are guided by the desire to remove oscillations from the jump contours. This is generally accomplished by factoring the jump matrix and deforming the contours so that each factor is isolated near saddle points, away from which they approach the identity exponentially fast.

To remove oscillations from the jump matrix, we need to examine the exponential that appears in these expressions, which we represent as $\exp\theta(k)$, where $\theta(k) = 2ikx + 8ik^3t$. As in the method of steepest descent for integrals, we deform the RHP through the saddle points of θ. We find that $\theta'(k) = 2ix + 24ik^2t$, and solving for $\theta'(k) = 0$ gives the saddle points $k = \pm k_0$, with $k_0 = \sqrt{-x/(12t)}$. The directions of steepest descent, at $\pm k_0$ — along which the oscillations of the jump matrix become exponential decay — are given by

$$\theta_s^+ = 3\pi/4 \pm \pi/2,$$
$$\theta_s^- = \pi/4 \pm \pi/2.$$

3.2.1 The Dispersive Region

We present the full deformation from the initial RHP on the real line. We introduce two factorizations of the original jump matrix $G(k; x, t)$:

$$G(k; x, t) = M(k; x, t)P(k; x, t),$$

$$M(k; x, t) = \begin{pmatrix} 1 & -\rho(-k)e^{-\theta(k)} \\ 0 & 1 \end{pmatrix}, \quad P(k; x, t) = \begin{pmatrix} 1 & 0 \\ \rho(k)e^{\theta(k)} & 1 \end{pmatrix},$$

$$G(k; x, t) = L(k; x, t)D(k; x, t)U(k; x, t), \quad L(k; x, t) = \begin{pmatrix} 1 & 0 \\ \rho(k)e^{\theta(k)}/(1 - \rho(k)\rho(-k)) & 1 \end{pmatrix},$$

$$D(k) = \begin{pmatrix} 1 - \rho(k)\rho(-k) & 0 \\ 0 & 1/(1 - \rho(k)\rho(-k)) \end{pmatrix}, \quad U(k; x, t) = \begin{pmatrix} 1 & -\rho(-k)e^{-\theta(k)}/(1 - \rho(k)\rho(-k)) \\ 0 & 1 \end{pmatrix}.$$

In what follows, we often suppress x and t dependence for notational simplicity. The factorizations are suggestively defined. M (for 'minus') will be deformed into the lower half-plane and P (for 'plus') will be deformed into the upper half-plane. L is lower triangular and will be deformed into the lower half-plane, D is diagonal and will not be deformed. Finally, U is upper triangular and will be deformed into the upper half-plane. Since $q \in \mathcal{S}_\delta(\mathbb{R})$ for some $\delta > 0$, ρ has an analytic continuation off the real line so that all the deformations are justified [13, 14]. These factorizations are used so that only one of $\exp\theta(k)$ or $\exp(-\theta(k))$ is present in each matrix. This makes it possible to deform the contours to new contours which have angles $\theta_s^\pm$ with the real axis, along which the jump matrices approach the identity exponentially fast. The 'ghost' contours introduced in Figure 5(a) all satisfy this desired property, and hence we define a new matrix function $\Phi_{2,d}$ based on these regions. Notice that the new definitions still satisfy the condition at infinity. We compute the jumps that $\Phi_{2,d}$ satisfies to phrase a RHP for $\Phi_{2,d}$, see Figure 5(b). This process is referred to as 'lensing' and is presented in more detail in Appendix A.

In order to achieve asymptotic stability we need the jump matrix to approach the identity away from $\pm k_0$, i.e., we need to remove the contour on $(-k_0, k_0)$. Indeed, numerical results show that the solution on this contour is increasingly oscillatory as $|x| + |t|$ become large. We introduce the unique 2×2 matrix-valued function Δ that satisfies the diagonal RHP

$$\Delta^+(k) = \Delta^-(k)D(k), \quad k \in (-k_0, k_0), \quad \Delta(\infty) = I. \tag{3.2}$$

See Appendix B for the exact form of Δ. Notice that in general Δ has singularities at $\pm k_0$. To combat this issue we introduce circles around both $\pm k_0$, see Figure 5(c). We define $\Phi_{3,d}$ by the definitions in Figure 6(a) where $\Phi_{3,d} = \Phi_{2,d}$ when no definition is specified. Computing the jumps we see that $\Phi_{3,d}$ satisfies the RHP in Figure 6(b). We apply the same procedure at $-k_0$ and obtain the problem shown graphically in Figure 7(a). Finally, we define $\Phi_{4,d} = \Phi_{3,d}\Delta^{-1}$ and $\Phi_{4,d}$ satisfies the RHP shown in Figure 7(b). We solve this resulting RHP numerically.

Remark 3.1. To obtain a RHP valid for $t = 0$ and $x < 0$ one can take the limit of the above RHP as $t \to 0^+$. In this limit $k_0 \to \infty$ and Δ has a jump on all of $\mathbb{R}$.

3.2.2 The Painlevé Region

For $x > 0$ this region intersects with the soliton region defined below, and we use that deformation. For $x < 0$, the saddle points are coalescing and this allows for a new deformation. In this region we reduce the number of contours present, in order to reduce the overall computational cost. Indeed, consider the interval between the two saddle points $[-k_0, k_0]$, where

$$|k| \leq \sqrt{\frac{C}{12}} t^{-1/3} \Rightarrow |2kx + 8k^3 t| \leq 2Ct^{1/3}k + 8k^3 t \leq \frac{2}{\sqrt{12}}C + \frac{8}{12\sqrt{12}}C^{3/2}.$$

This implies that the oscillations are controlled between the two saddle points and the LDU factorization is not needed. See Figure 8(a) for the RHP in this region.
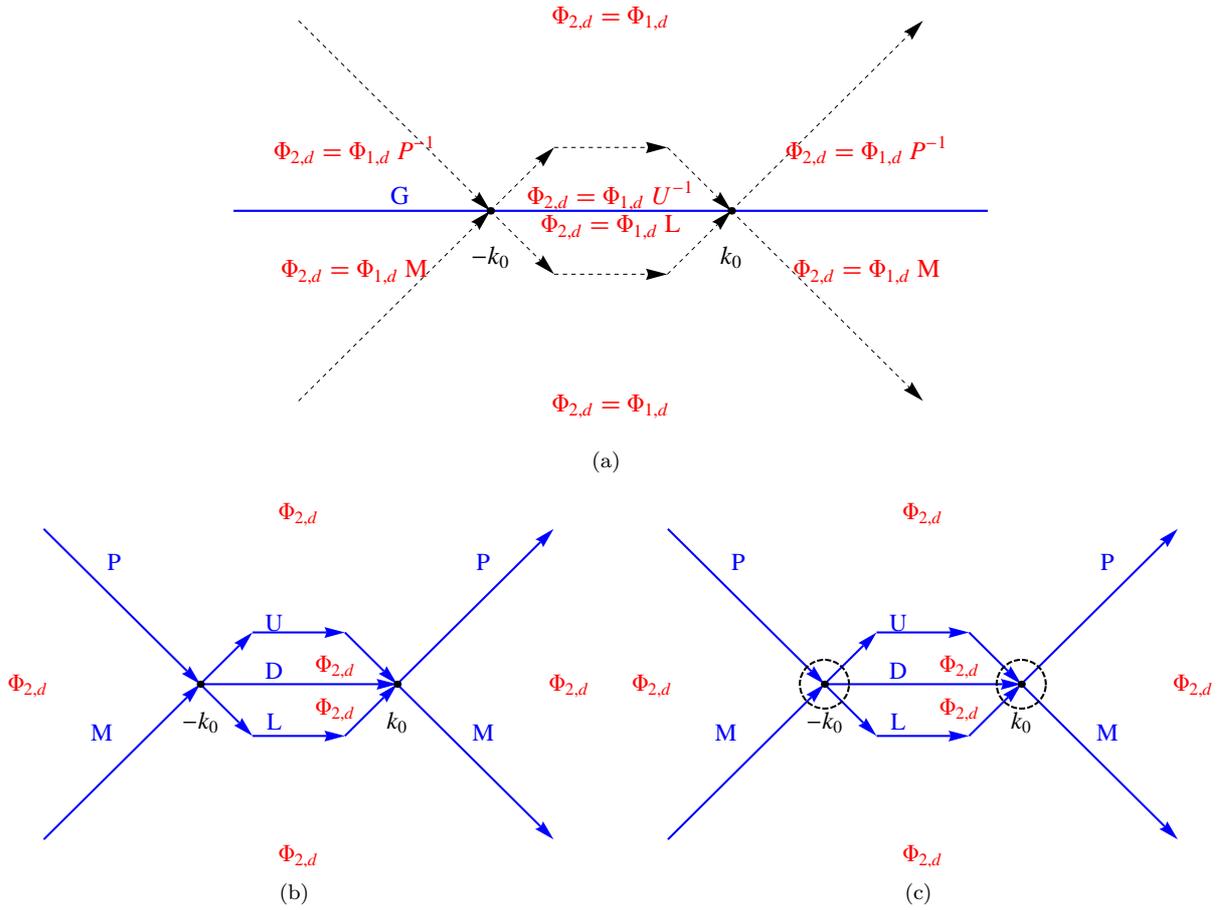
Figure 5: (a) The jump contours and matrices of the initial RHP with 'ghost' contours, (b) Graphical representation of the jump contours and matrices of the RHP satisfied by $\Phi_{2,d}$, (c) Ghost circles in preparation for the singularities of Δ.

Remark 3.2. The deformations for the dispersive region and the Painlevé regions are valid in overlapping regions of the (x,t)-plane. As $x \to 0, x < 0$, the deformation for the dispersive region can be used until the Painlevé region is reached. Using these deformations in tandem allows the method to retain accuracy in the region $x < 0$, $t \geq 0$ for $|x|$ and t large. Note that for the deformation for the dispersive region to be valid as $k_0 \to 0$ it is necessary that $\|\rho\|_\infty < 1$ because of the form of D.

3.2.3   The Soliton Region

Choose a function $\alpha(x,t)$ so that $0 \leq \alpha(x,t) < \sqrt{3}|k_0|$, then the deformation used in this region is given in Figure 8(b). Note that the angle of the contours is chosen so that $\operatorname{Re}\theta(k) \leq 0$ on all contours with $\operatorname{Im} k > 0$, whereas $\operatorname{Re}\theta(k) > 0$ on all contours with $\operatorname{Im} k \leq 0$.

Remark 3.3. There is a lot of freedom in choosing α. For simplicity, we assume the reflection coefficient is analytic and decays in the strip $\{s + ti : s \in \mathbb{R}, \ t \in (-T, T), \ T > 0.5\}$, and therefore we use $\alpha(x,t) = \min\{.5, \sqrt{3}k_0\}$.

3.3   Numerical Results

There are additional issues that have to be addressed before these RHPs can be efficiently solved numerically. First, in §3.2.1 we opened up circles around two singularities at $\pm k_0$. This deformation is valid provided the
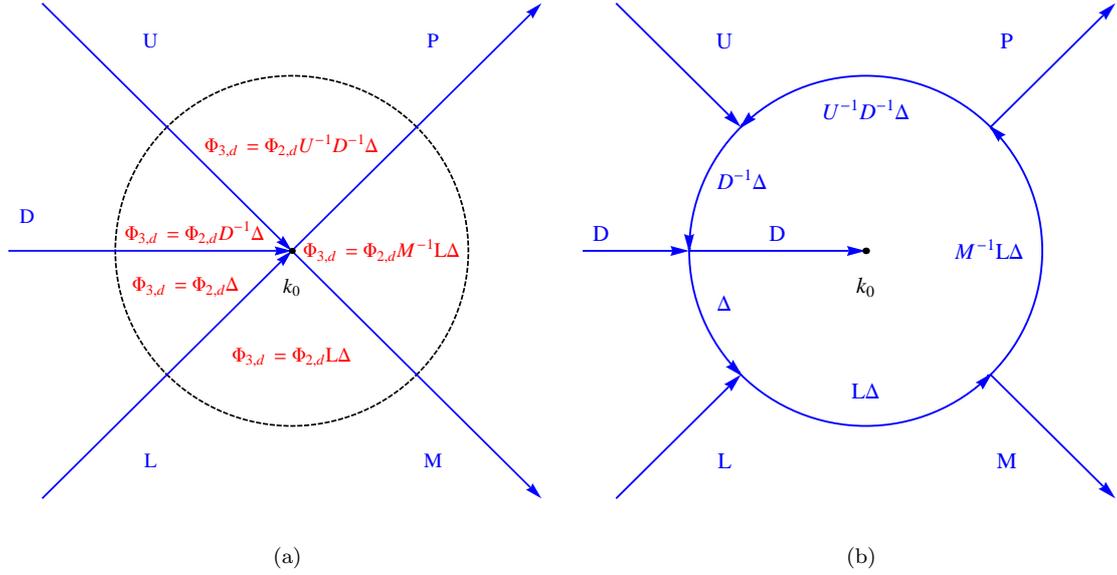
Figure 6: (a) Definition of $\Phi_{3,d}$ near k_0, (b) The jump contours and matrices of the RHP satisfied by $\Phi_{3,d}$ near k_0.

radius of the circles is sufficiently small. In addition, we need to shrink the radius of these circles if $|x|$ or t is large. We use the following rule of thumb. Assume the saddle point is at zero and a parametrix has introduced a singularity at zero. Further assume the oscillator is $\exp(wk^r)$, $r > 1$, where w is a parameter. We scale the radius like $w^{-1/r}$ as w becomes large. This ensures oscillations are controlled on the circle while maintaining some distance from the singularity. Second, we truncate contours when the jump matrices are to machine precision, the identity matrix. This allows us to have only finite contours present in the problem. Furthermore, it allows the contours to shrink as x and t increase, since the exponential decay is more drastic. The scaling on these contours is the same as for the circles around the saddle points. Note that if all jump contours are decaying to the identity as x and t becomes large, it is possible that we truncate all contours and approximate the solution by zero.

Finally, we define $q(n, x, t)$ as the approximation to the solution of mKdV with n collocation points on each contour where the initial condition is implied from context.

3.3.1 Direct Scattering

For an initial condition where the reflection coefficient is not known explicitly we can verify our direct, and in the process, inverse scattering computations by evaluating the solution to the inverse problem at $t = 0$. As an example we start with the initial condition $q(x, 0) = -1.3 \operatorname{sech}^2(x)$. In Figure 9 we plot the error, $|q(x, 0) - q(80, x, 0)|$, while varying the number of collocation points.

3.3.2 Inverse Scattering

Throughout this section we assume that the reflection coefficient is obtained to machine precision.

1. *Convergence.* To analyze the error we introduce some notation. Define

$$Q_n^m(x, t) = |q(n, x, t) - q(m, x, t)|.$$

Using this notation, see Figure 24 for a demonstration of spectral (Cauchy) convergence with each of the deformations.
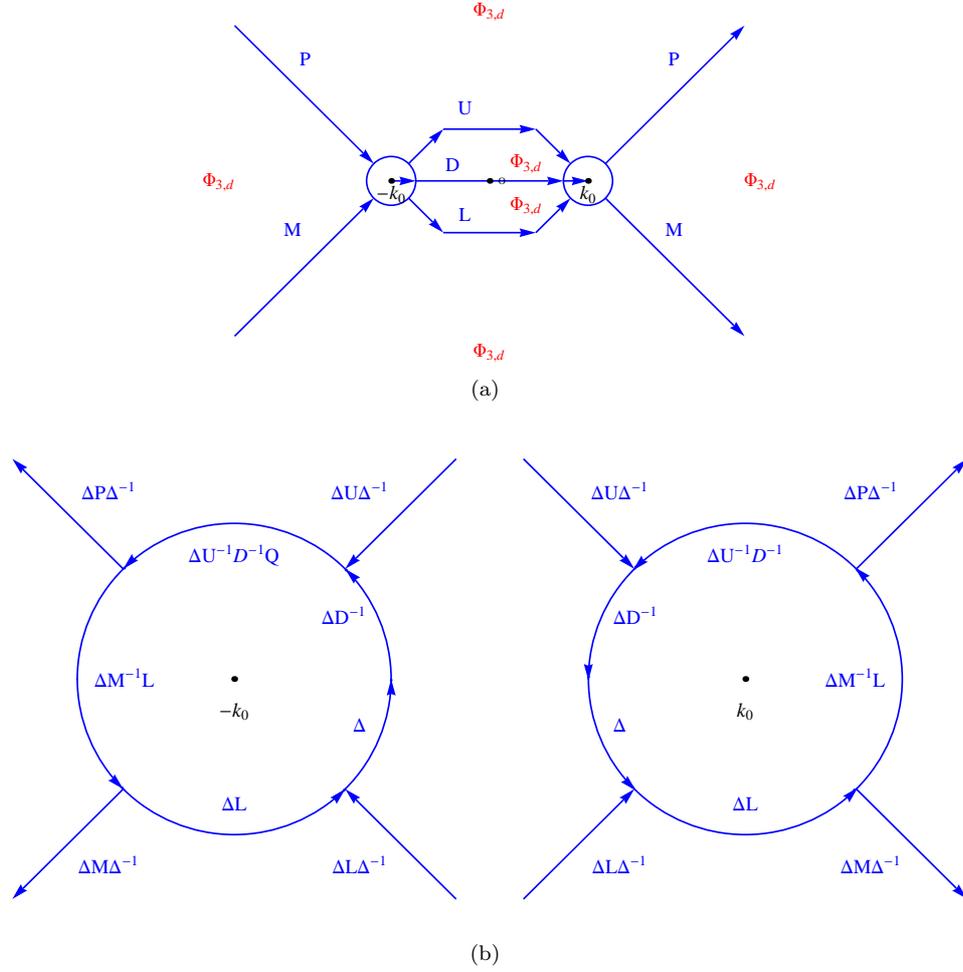
Figure 7: (a) The jump contours and matrices of the RHP satisfied by $\Phi_{3,d}$, (b) The jump contours and matrices of the RHP satisfied by $\Phi_{4,d}$. Note that the contours with jumps $\Delta U \Delta^{-1}$ and $\Delta L \Delta^{-1}$ connect.

2. *Asymptotic Stability.* For the method to be asymptotically stable we require that, for a given n and m, $Q_n^m(x,t)$ remains bounded (and small) as $|x| + |t|$ becomes large. In fact, what we numerically demonstrate is that $Q_n^m(x,t)$ tends to zero in all regions. See Figure 11 for the demonstration of this.

3.3.3 Comparison with Asymptotic Formulae

In §2.4.1 asymptotic formulae in various regions for mKdV were presented. In this section we compare numerical results with these formulae. We skip the soliton region because the asymptotic formula approximates the solution by zero, which is uninteresting. Taking into account the verifiable convergence, we note that the computed solutions in the plots below are closer to the true solution than the asymptotic formulae.

1. *The Dispersive Region.* In Figure 12 we present a numerical verification of the error bound (2.14) along with a plot of both approximations in the dispersive region.

2. *The Painlevé Region.* In Figure 12 we present a numerical verification of the error bound (2.12) along with a plot of both approximations in the Painlevé region.

With minimal deformations we obtain a numerical method for defocusing mKdV that is not only asymptotically accurate but also converges spectrally fast. The roles of x and t are reduced to that of parameters
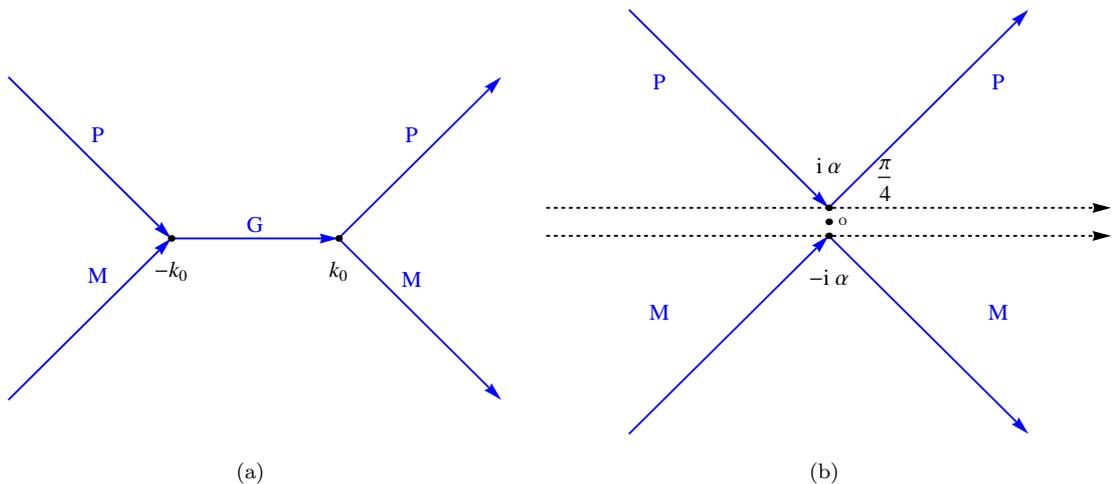
Figure 8: (a) The jump contours and matrices of the RHP for mKdV in the Painlevé region with $x < 0$. (b) The jump contours and matrices of the RHP for mKdV in the soliton region.
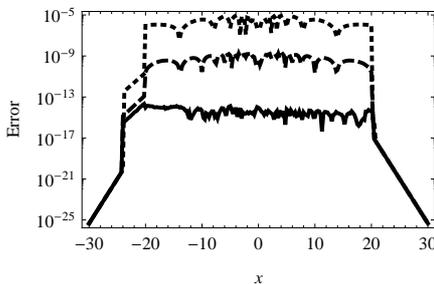

Figure 9: Error in performing the full inverse scattering transformation at $t = 0$ while varying the number of collocation points, m, for the direct scattering. ($m = 20$: dotted line, $m = 40$: dashed line, $m = 80$: solid line.) Note that for moderate $|x|$ we approximate $q(x,0)$ by zero after the truncating contours and obtain very small absolute error.

and we have no need for spatial grids or time-stepping. The dispersive nature of mKdV is captured exactly. The amount of effort required to solve mKdV should be typical when considering other integrable equations with Riemann–Hilbert formulations. Below we solve KdV and in the process expand the scope of the numerical method to deal with RHPs that have singularities. This complication is not typical but we proceed to show that it can be dealt with.

4   The Korteweg–de Vries Equation

We discuss numerical inverse scattering for KdV. We can adjust the constants c_j in §2.4.2 to make the dispersive region overlap with the Painlevé region up to some finite t. This essentially allows one to use only the deformations needed for mKdV with minor alterations. For practical purposes this is sufficient. Since we are interested in the development of an asymptotically stable method, we need to construct significantly more complicated deformations.

The RHP for KdV is generally a meromorphic problem which alters the deformations for $x > 0$. Additionally, $\rho(0) = -1$, generically, which complicates the deformations for $x < 0$. The deformation for the dispersive region is only stable in its original region of definition, $-x > \alpha t$, $\alpha > 0$; it cannot be extended into the Painlevé region for large t. For concreteness we use $-x > 12t > 0$. As a consequence, the three regions defined in the case of mKdV do not overlap for KdV. To overcome this issue Deift, Zhou and Venakides
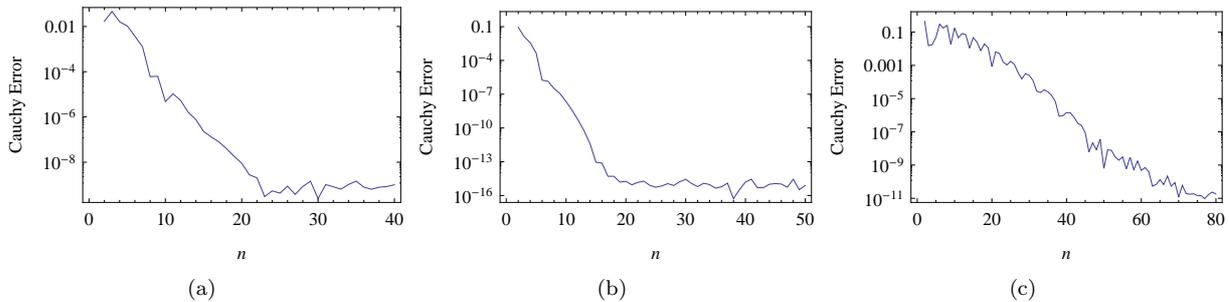
Figure 10: Demonstration of spectral convergence for mKdV with $q(x,0) = -1.3 \operatorname{sech}^2(x)$. All plots have $Q_{2m}^n(x,t)$ plotted as a function of n as n ranges from 2 to m. (a) Dispersive Region: $m = 40$ at the point $(x,t) = (-8.8, 0.6)$, (b) Painlevé Region: $m = 50$ at the point $(x,t) = (-0.8, 0.6)$, (c) Soliton/Painlevé Region: $m = 100$ at the point $(x,t) = (0.2, 2.6)$. This deformation requires more collocation points because it only has four contours, so that each contour contains more information about the solution.

used a new deformation of the RHP for the collisionless shock region [7] (see [18] for the first appearance of this region). This deformation is valid into the dispersive region but does not extend to the Painlevé region. Below we present the deformations for the RHP associated with KdV in these four classical regions. To fill the final gap we introduce a new deformation to transition from the collisionless shock region into the Painlevé region.

4.1 Numerical Computation of the Scattering Data for KdV

Calculating the scattering data numerically relies on two spectral methods: a Chebyshev collocation method for ODEs and Hill's method [19] for computing the spectrum of a linear operator.

- Computing ρ.

  For $k \in \mathbb{R}$ we are looking for solutions of $\mu_{xx} + q_0(x)\mu = -k^2\mu$ which behave like $\exp(\pm ikx)$ as $x \to \pm\infty$. If $q_0(x) \in \mathcal{S}_\gamma(\mathbb{R})$ the eigenfunctions limit to this asymptotic behavior exponentially fast. For illustration purposes we concentrate on the eigenfunctions at $-\infty$. We set $u(x) = \mu(x)e^{\mp ikx} - 1$ where the $\pm$ is chosen when $\mu \backsim e^{\mp ikx}$. Then $u(x)$ satisfies the ODE

  $$u_{xx} \mp 2iku_x + q_0(u+1) = 0, \quad u(-\infty) = u'(-\infty) = 0.$$

  A Chebyshev collocation method is used to solve this equation on $(-\infty, 0]$ for each choice of $\pm$. The same ideas apply to the eigenfunctions whose behavior is specified at $+\infty$. We solve for these on $[0, \infty)$. As in the case of mKdV, matching the solutions at the origin produces the reflection coefficient.

  Remark 4.1. It should be possible to use GMRES [20] on this problem to develop a fast method, as in [21].

- Computing $\{\kappa_1, \ldots, \kappa_n\}$.

  Calculating these values is equivalent to calculating the $L^2(\mathbb{R})$ eigenvalues of the operator $\partial_x^2 + q_0(x)$ [14]. Through the transformation $x = 2\tan(y/2)$ we map the original ODE to the interval $[-\pi, \pi]$. This is well-defined because of the decay of q_0. If $m(y) = \mu(2\tan(y/2))$ and $Q(y) = q_0(2\tan(y/2))$, then m satisfies the problem

  $$\cos^2(y/2)\left(\cos^2(y/2)m_y\right)_y + Q(y)m = \lambda m, \quad \lambda = -k^2, \quad m(x) = m(x+\pi). \tag{4.1}$$

  Define $C_p^k([a,b]) = \{f \in C^k([a,b]) : f^{(j)}(a) = f^{(j)}(b), \quad 0 \le j \le k\}$. To show the equivalence of this problem with solving the original scattering problem we have the following lemma.
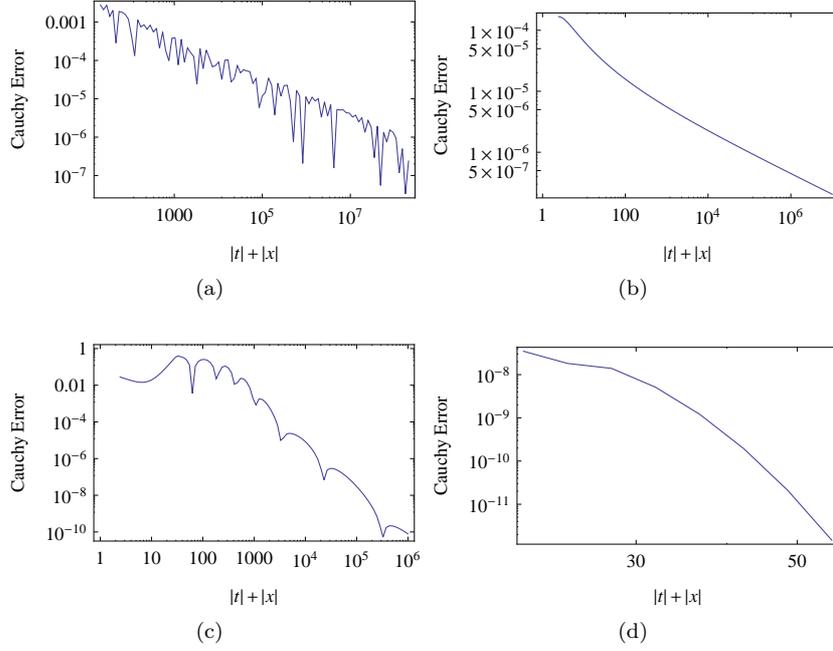
Figure 11: Demonstration of asymptotic stability for mKdV with $q(x,0) = -1.3 \operatorname{sech}(x)^2$. All plots have $Q_m^n(x,t)$ plotted as a function of $|t| + |x|$. (a) *The Dispersive Region*: $m = 10$, $n = 5$ along the trajectory $x = -20t$, (b) *The Painlevé Region*: $m = 10$, $n = 5$ along the trajectory $x = -(3t)^{1/3}$, (c) *The Painlevé Region*: $m = 20$, $n = 10$ along the trajectory $x = (3t)^{1/3}$, (d) *The Soliton Region*: $m = 10$, $n = 5$ along the trajectory $x = 20t$.

Lemma 4.1. Assume $q_0(x) \in \mathcal{S}(\mathbb{R})$ and $m \in C_p^2([-\pi, \pi])$ solves (4.1) with $\lambda > 0$ then $\mu(x) = m(2 \arctan(x/2))$ is an L^2 eigenfunction of $\partial_x^2 + q_0(x)$. Furthermore, all L^2 eigenfunctions for $\partial_x^2 + q_0(x)$ can be found this way.

Proof. The behavior of the coefficients of (4.1) at $\pm\pi$ forces $m(\pm\pi) = 0$. Also, m is Lipschitz with constant $C = \sup_{y \in [-\pi,\pi]} |m'(y)|$. Therefore

$$|m(y) - m(\pm\pi)| \leq C|y \mp \pi| \Rightarrow |m(y)| \leq C|y \mp \pi|.$$

Using the asymptotic expansion of $2 \arctan(x/2)$ we see that

$$|\mu(x)| \leq \min\{C|2 \arctan(x/2) - \pi|, C|2 \arctan(x/2) + \pi|\} \leq C'/(1 + |x|)$$

for a new constant C'. This shows μ is an L^2 eigenfunction. Now assume that μ is an L^2 eigenfunction of the operator $\partial_x^2 + q_0(x)$. We know that $\lambda > 0$ and $\mu \backsim \exp(-\sqrt{\lambda}|x|)$ as $|x| \to \infty$ [14]. Since q is smooth μ must be smooth and $\mu(2 \tan(y/2))$ is a $C_p^2([-\pi, \pi])$ solution of (4.1). Therefore these eigenvalues and eigenfunctions are in direct correspondence. ∎

Applying the techniques in [19] to (4.1) allows us to obtain $\{\kappa_1, \ldots, \kappa_n\}$ with spectral accuracy.

- Computing $\{C_1, \ldots, C_n\}$.

  As mentioned above, all poles of $\rho(k) = b(k)/a(k)$ are simple. Since the above method for calculating $\rho(k)$ gives a method for computing $b(k)$ we reduce the problem to computing $a'(\kappa_j)$. We use the
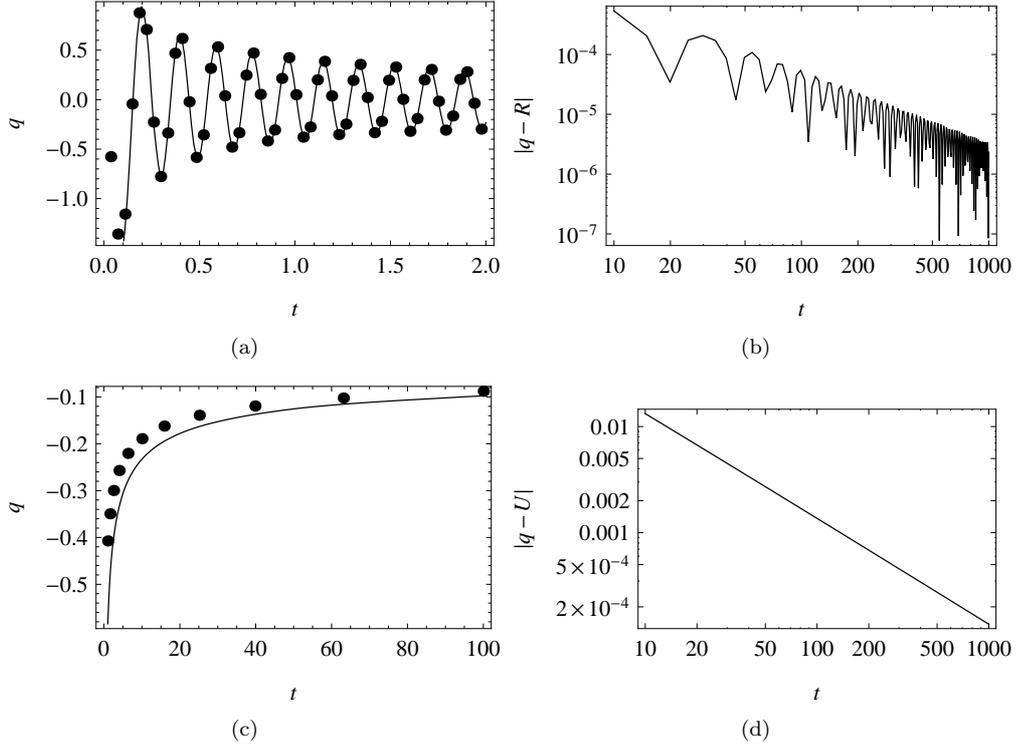
Figure 12: Comparison of numerical results with the asymptotic formulae in the dispersive and Painlevé regions for mKdV. (a) *The Dispersive Region:* $q(10, x, t)$ and $R(x, t)$ plotted as a function of t with $x = -20t$. The computed solution is shown by the solid line and the asymptotic formula by the dots, (b) *The Dispersive Region:* $|q(10, x, t) - R(x, t)|$ plotted as a function of t with $x = -20t$. A least-squares fit gives $|q(10, x, t) - R(x, t)| = \mathcal{O}(t^{-1.2})$, in agreement with the error formula, (c) *The Painlevé Region:* $q(10, x, t)$ and $U(x, t)$ plotted as a function of t with $x = -t^{1/3}$. The computed solution is shown by the solid line and the asymptotic formula by dots, (d) *The Painlevé Region:* $|q(10, x, t) - U(x, t)|$ plotted as a function of t with $x = -t^{1/3}$. A least-squares fit gives $|q(10, x, t) - U(x, t)| = \mathcal{O}(t^{-0.65})$, in agreement with the error formula.

relationship [14]

$$a'(\kappa_j) = \frac{1}{ib(\kappa_j)} \int_{\mathbb{R}} \mu(x; \kappa_j)^2 dx,$$

where μ is the eigenfunction of the operator $\partial_x + q_0(x)$ with eigenvalue $\lambda = \kappa_j^2$ such that $\mu \backsim \exp(-|\lambda x|)$ as $|x| \to \infty$. This is evaluated using Clenshaw–Curtis quadrature.

4.2 Numerical Solution of the Inverse Problem

4.2.1 The Dispersive Region

We proceed as in the case of mKdV. Assume we performed the deformation in Remark 2.6 to introduce small circles around each pole. Examining the exponent, $\exp(2i\kappa_j x + 8i\kappa_j^3 t)$, and further recalling that $\kappa_j \in i\mathbb{R}^+$,

we see that the exponent is unbounded in this region. Following the approach in [8] we define

$$
\Phi_{1,d}(k;x,t) = \begin{cases}
\Phi(k;x,t)\begin{pmatrix} 1 & -(k-\kappa_j)/(C_j e^{\theta(k_0)}) \\ C_j e^{\theta(k_0)}/(k-\kappa_j) & 0 \end{pmatrix} Q(k), & \text{if } |k-\kappa_j| < \epsilon, \\[12pt]
\Phi(k;x,t)\begin{pmatrix} 0 & -C_j e^{\theta(k_0)}/(k+\kappa_j) \\ (k+\kappa_j)/(C_j e^{\theta(k_0)}) & 0 \end{pmatrix} Q(k), & \text{if } |k+\kappa_j| < \epsilon, \\[12pt]
\Phi(k;x,t)Q(k), & \text{otherwise,}
\end{cases}
$$

for

$$
Q(k) = \begin{pmatrix} \prod_{j=0}^n (k-\kappa_j)/(k+\kappa_j) & 0 \\ 0 & \prod_{j=0}^n (k+\kappa_j)/(k-\kappa_j) \end{pmatrix}.
$$

Note that the matrix

$$
\begin{pmatrix} 1 & -(k-\kappa_j)/(C_j e^{\theta(k_0)}) \\ C_j e^{\theta(k_0)}/(k-\kappa_j) & 0 \end{pmatrix} Q(k),
$$

has a removable pole at κ_j and $\Phi_{1,d}$ still tends to the identity at infinity. Recall $A_j^\pm = \{k \in \mathbb{C} : |k \mp \kappa_j| = \epsilon\}$ where Aj^+ has counter-clockwise orientation, and A_j^- clockwise. Further ϵ is chosen small enough so that the $A_j^\pm$ do not intersect any other contour. We compute the jumps of $\Phi_{1,d}$:

$$
\Phi_{1,d}^+(k;x,t) = \begin{cases}
\Phi_{1,d}^-(k;x,t)Q^{-1}GQ(k;x,t), & \text{if } k \in \mathbb{R}, \\[12pt]
\Phi_{1,d}^-(k;x,t)Q^{-1}(k)\begin{pmatrix} 1 & -(k-\kappa_j)/(C_j e^{\theta(k_0)}) \\ 0 & 1 \end{pmatrix} Q(k), & \text{if } k \in A_j^+, \\[12pt]
\Phi_{1,d}^-(k;x,t)Q^{-1}(k)\begin{pmatrix} 1 & 0 \\ -(k+\kappa_j)/(C_j e^{\theta(k_0)}) & 1 \end{pmatrix} Q(k), & \text{if } k \in A_j^-,
\end{cases}
$$

$$
\Phi_{1,d}(\infty;x,t) = \begin{pmatrix} 1 & 1 \end{pmatrix}.
$$

This effectively inverts the exponent and turns exponential blowup into decay to the identity. This demonstrates that the solitons exhibit exponential decay. To simplify the notation, define

$$
T_+(k,j;x,t) = \begin{pmatrix} 1 & 0 \\ -C_j e^{\theta(\kappa_j)}/(k-\kappa_j) & 1 \end{pmatrix}, \quad T_-(k,j;x,t) = \begin{pmatrix} 1 & -C_j e^{\theta(\kappa_j)}/(k+\kappa_j) \\ 0 & 1 \end{pmatrix},
$$

$$
S_+(k,j;x,t) = \begin{pmatrix} 1 & -(k-\kappa_j)/(C_j e^{\theta(\kappa_j)}) \\ 0 & 1 \end{pmatrix}, \quad S_-(k,j;x,t) = \begin{pmatrix} 1 & 0 \\ -(k+\kappa_j)/(C_j e^{\theta(\kappa_j)}) & 1 \end{pmatrix}.
$$

As before, the 'ghost' contours introduced in Figure 13(a) pass along the directions of steepest descent. We define a new matrix function $\Phi_{2,d}$ based on these regions. Notice that the new definitions still satisfy the normalization condition at infinity. We compute the jumps that $\Phi_{2,d}$ satisfies to phrase a RHP for $\Phi_{2,d}$, see Figure 13(b). Throughout the figures in this section, the dot inside the circles with jumps $T_\pm$ or $S_\pm$ represent $\pm\kappa_j$.

We decompose G into its LDU and MP factorizations and deform the jump contour off $\mathbb{R}$ as we did in §3.2.1. However, there is a significant difference: if we examine the matrix D, we see that there is a singularity at the origin, since generically $\rho(0) = -1$ [14]. We need to remove this singularity in order to represent the solution by Chebyshev polynomials. Additionally, we need to remove the contour on $(-k_0, k_0)$ to attain asymptotic stability as mentioned in §3.2.1 using Δ in Appendix B. We proceed in the same way and arrive at the RHP in Figure 14, noting that the circles (corresponding to solitons) and presence of the matrix Q are the only aspects that are different.

Remark 4.2. We assumed that $\rho(0) = -1$. If it happens that $|\rho(0)| < 1$ then the deformations reduce to those done for mKdV but now in the (possible) presence of solitons. Numerical results show that this can happen when an initial condition for KdV is obtained through the Miura transformation, see §4.4. In this case, the deformations for the dispersive, Painlevé and soliton regions cover the (x,t)-plane.
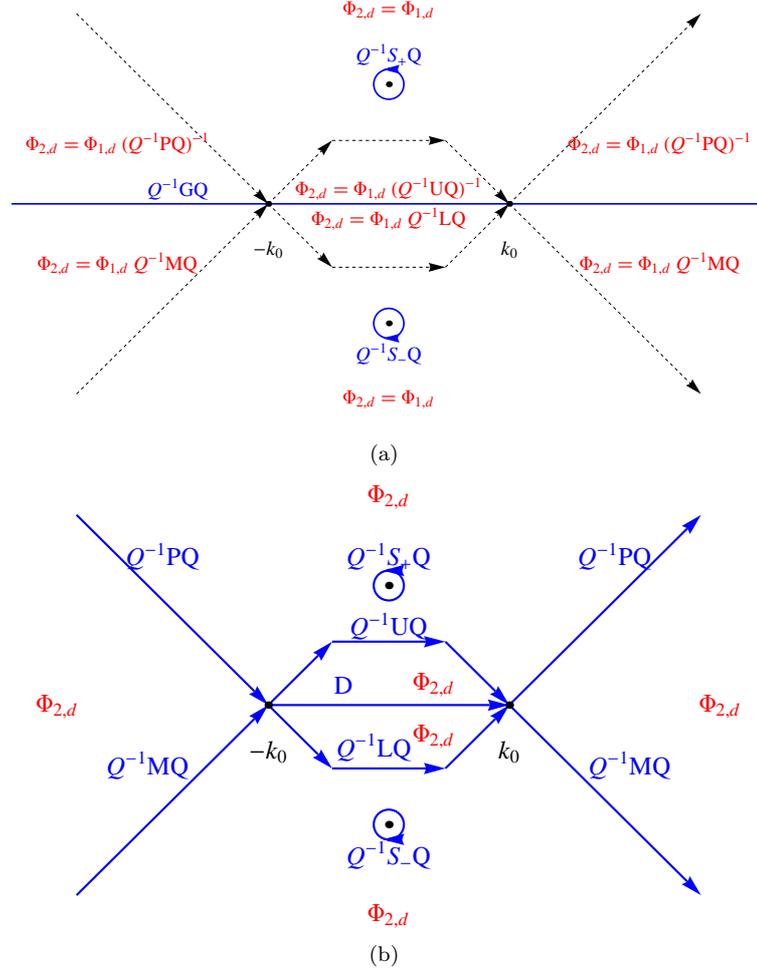
Figure 13: (a) Jump contours and matrices for the initial RHP with 'ghost' contours, (b) Jump contours and matrices for the RHP satisfied by $\Phi_{2,d}$.

4.2.2 The Painlevé Region

As in the case of mKdV, for $x > 0$ we have an intersection with the soliton region defined below. We use that deformation. The final deformation for KdV when $x < 0$ is nearly the same as in the case of mKdV, see Figure 15.

4.2.3 The Collisionless Shock Region

The singularity at $k = 0$ in the matrix $D(k)$ destroys the boundedness of $\Delta(k)$ which poses problems that do not occur for mKdV. As $k \to 0$ the matrices $\Delta Q^{-1} P Q \Delta^{-1}$ and $\Delta Q^{-1} M Q \Delta^{-1}$ are unbounded and we cannot link up the dispersive region with the Painlevé region, as we did for mKdV. By choosing C large we can make the dispersive and Painlevé regions overlap up to some finite t. We wish to obtain a method which is stable for large t. We need to introduce additional deformations to bridge the dispersive and Painlevé regions. The first region we address is the collisionless shock region. Ablowitz and Segur [18] introduced this region, and Deift et al. produced explicit asymptotics [7].

The results presented below for this region are from [7]. As x increases in the dispersive region, the stationary points of $\exp\theta$, $\pm k_0$, approach the singularity ($k = 0$) of the parametrix Δ. To prevent this, we replace θ by a so-called g function [22], whose stationary points, after scaling, do not approach a singularity.
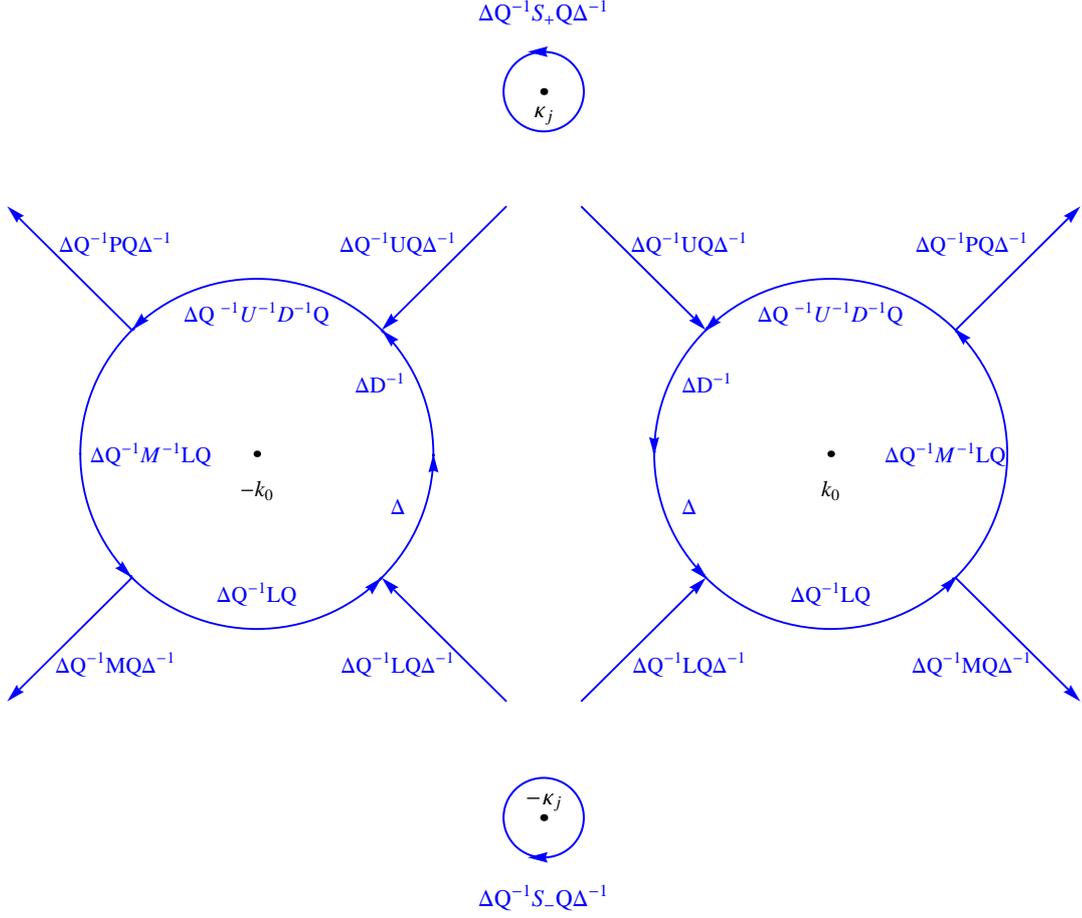
Figure 14: A zoomed view of the jump contours and matrices for the RHP in the dispersive region of KdV. Note that the contours with jumps $\Delta Q^{-1}UQ\Delta^1$ and $\Delta Q^{-1}LQ\Delta^1$ connect.

For $b > a > 0$, we determine constants D_1, D_2 so that there exists a function $g(k; x, t)$ which is bounded in the finite plane and satisfies the following properties:

$$g^-(k; x, t) + g^-(k; x, t) = \begin{cases} D_1 & \text{if } k \in (-b, -a), \\ -D_1 & \text{if } k \in (a, b), \end{cases}$$

$$g^+(k; x, t) - g^-(k; x, t) = D_2, \quad k \in (-a, a),$$

$$g(k; x, t) \text{ analytic in } k \text{ off } [-b, b],$$

$$g(k; x, t) \text{ has stationary points at } \pm(a, b),$$

$$g(k; x, t) \backsim 4k^3 - 12k \text{ as } k \to \infty.$$

The constants D_1 and D_2 depend on a and b and have desired properties to scale away singularities. These will be determined below. Also, once all these constants are fixed, g is uniquely determined.

Remark 4.3. For KdV, g can be determined explicitly (Appendix C) but it is more instructive to introduce it as above. It is more convenient to compute it numerically from this formulation since the method in [23] can easily be adapted to ensure spectral accuracy.
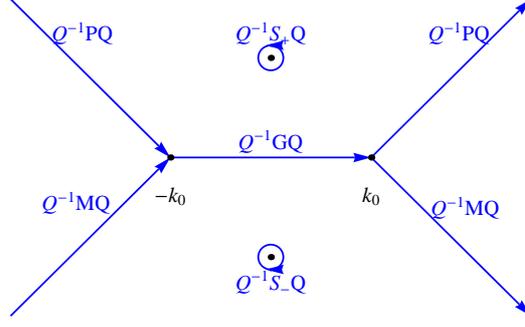
Figure 15: The jump contours and matrices for the RHP in the Painlevé Region with $x < 0$.

Define the function $\gamma(k) = -i\tau[4k^3 - 12k - g(k)]$, $\tau = tk_0^3$ and construct

$$\phi(k) = \begin{pmatrix} e^{\gamma(k)} & 0 \\ 0 & e^{-\gamma(k)} \end{pmatrix} \to I \text{ as } k \to \infty.$$

It is advantageous to introduce a scaling operator, $\frown$, defined by $\tilde{f}(\cdot; x, t) = f(k_0\cdot; x, t)$ and solve for $\tilde{\Phi}(k; x, t)$. For $k \in \mathbb{R}$ the jump satisfied by $\tilde{\Phi}(k; x, t)\phi(k)$ is $\phi_-^{-1}(k)\tilde{G}(k; x, t)\phi_+(k)$. This assumes the absence of solitons, otherwise we replace G by $Q^{-1}GQ$. Explicitly

$$\phi_-^{-1}(k)\tilde{G}(k; x, t)\phi_+(k) = \begin{pmatrix} [1 - \rho(k_0k)\rho(-k_0k)]e^{\gamma^+(k) - \gamma^-(k)} & -\rho(-k_0k)e^{-\theta(k_0k) - \gamma^+(k) - \gamma^-(k)} \\ \rho(k_0k)e^{\theta(k_0k) + \gamma^+(k) + \gamma^-(k)} & e^{-\gamma^+(k) + \gamma^-(k)} \end{pmatrix}.$$

Note that $\theta(k_0k) = 2ik_0kx + 8ik_0^3k^3t = 2i\tau(-12k + 4k^3)$, and γ satisfies

$$\begin{aligned} \gamma^+(k) - \gamma^-(k) &= i\tau(g^+(k) - g^-(k)) = 0 \text{ for } k \notin [-b, b], \\ \gamma^+(k) + \gamma^-(k) &= i\tau(g^+(k) + g^-(k)) - \theta(k_0k) \to 0 \text{ as } k \to \infty. \end{aligned}$$

We write

$$\phi_-^{-1}(k)\tilde{G}(k; x, t)\phi(k)_+ = \begin{cases} \begin{pmatrix} 1 - \rho(k_0k)\rho(-k_0k) & -\rho(-k_0k)e^{2i\tau g(k)} \\ \rho(k_0k)e^{2i\tau g(k)} & 1 \end{pmatrix}, & \text{if } k \in (-\infty, -b), \\[2em] \begin{pmatrix} [1 - \rho(k_0k)\rho(-k_0k)]e^{i\tau(g^+(k) - g^-(k))} & -\rho(-k_0k)e^{-C_1} \\ \rho(k_0k)e^{C_1} & e^{i\tau(-g^+(k) + g^-(k))} \end{pmatrix}, & \text{if } k \in (-b, -a), \\[2em] \begin{pmatrix} [1 - \rho(k_0k)\rho(-k_0k)]e^{C_2} & -\rho(-k_0k)e^{i\tau(-g^+(k) - g^-(k))} \\ \rho(k_0k)e^{i\tau(g^+(k) + g^-(k))} & e^{-C_2} \end{pmatrix}, & \text{if } k \in [-a, a], \\[2em] \begin{pmatrix} [1 - \rho(k_0k)\rho(-k_0k)]e^{i\tau(g^+(k) - g^-(k))} & -\rho(-k_0k)e^{C_1} \\ \rho(k_0k)e^{C_1} & e^{i\tau(-g^+(k) + g^-(k))} \end{pmatrix}, & \text{if } k \in (a, b), \\[2em] \begin{pmatrix} 1 - \rho(k_0k)\rho(-k_0k) & -\rho(-k_0k)e^{-2i\tau g(k)} \\ \rho(k_0k)e^{2i\tau g(k)} & 1 \end{pmatrix}, & \text{if } k \in [b, \infty), \end{cases}$$

(4.2)

where $C_1/i\tau = g^+(k) + g^-(k)$ for $k \in [a, b]$ and $C_2/i\tau = g^+(k) - g^-(k)$ for $k \in [-a, a]$. This successfully removes θ from the problem. As in the dispersive region, we proceed to factor $\tilde{G} = \tilde{L}\tilde{D}\tilde{U}$ on $[-a, a]$. Again, $\tilde{D}$ has a singularity at the origin that we must remove. Before we remove this singularity let us analyze the

24

system in the limit as $k_0 \to 0$ as this will guide the choice of the parametrix and the constants C_1 and C_2. On the interval $[-a, a]$ we have

$$\phi_-^{-1}(k)\tilde{D}(k)\phi_+(k) = \begin{pmatrix} [1 - \rho(k_0 k)\rho(-k_0 k)]e^{C_2} & 0 \\ 0 & ([1 - \rho(k_0 k)\rho(-k_0 k)]e^{C_2})^{-1} \end{pmatrix}.$$

Using $\rho(0) = -1$ and that ρ is analytic in a neighborhood of the origin we obtain that $1 - \rho(k_0 k)\rho(-k_0 k) = 2\nu k^2 k_0^2 + \mathcal{O}((kk_0)^4)$ near $k = 0$ for some constant ν. We left $b > a > 0$ mostly arbitrary above. It follows (Appendix C) that the boundedness condition along with the prescribed asymptotic behavior requires $a^2 + b^2 = 2$, leaving a single degree of freedom. We use this degree of freedom to enforce $k_0^2 \exp(C_2) = 1$, so that $(1 - \rho(k_0 k)\rho(-k_0 k)) \exp(C_2) \backsim 2\nu k^2 + \mathcal{O}(k_0^2 k^4)$. Removing, to second order, the dependence on k_0. To see that there does exist an a that satisfies this condition, we refer to the explicit construction of g in Appendix C. As $k, k_0 \to 0$ there is a constant $C > 1$ so that

$$\frac{1}{C} \le \frac{1 - \rho(k_0 k)\rho(-k_0 k)}{k^2} e^{C_2} \le C, \quad \text{for } k \in [-a, a].$$

Thus, to obtain a parametrix, we should solve the RHP

$$\psi_+(k) = \psi_-(k)\phi_-^{-1}(k)\tilde{D}(k)\phi^+(k), \quad k \in (-a, a), \quad \psi(\infty) = I.$$

This diagonal RHP can be solved explicitly using Appendix B. We conjugate the problem by ψ in the same way as was done with Δ in §4.2.1.

The full deformation for this region now follows. We lens the scaled problem into the form shown in Figure 16(a). Near a, b the jumps on the contours are also given there. Define $\Phi_{2,cs} = \Phi_{1,cs}\phi$. Near a, b, $\Phi_{2,cs}$ satisfies the problem shown in Figure 17. We conjugate by the parametrix, defining $\Phi_{3,cs} = \Phi_{2,cs}\psi^{-1}$. See Figure 17 for the RHP near a, b for $\Phi_{3,cs}$. By symmetry, what happens at $-a, -b$ is clear. More work is necessary. Define the two functions β_m and β_p via diagonal RHPs

$$\beta_m^+(k) = \beta_m^-(k)(\phi_-^{-1}\tilde{D}\phi_+)^{-1}, \quad k \in (-b, -a), \quad \beta_m(\infty) = I,$$
$$\beta_p^+(k) = \beta_p^-(k)(\phi_-^{-1}\tilde{D}\phi_+)^{-1}, \quad k \in (a, b), \quad \beta_m(\infty) = I.$$

For the final deformation define

$$\Phi_{4,cs} = \begin{cases} \Phi_{3,cs}\phi^{-1} & \text{inside the circle centered at } -b, \\ \Phi_{3,cs}\beta_m & \text{inside the circle centered at } -a, \\ \Phi_{3,cs}\beta_p & \text{inside the circle centered at } a, \\ \Phi_{3,cs}\phi^{-1} & \text{inside the circle centered at } b, \\ \Phi_{3,cs} & \text{otherwise.} \end{cases}$$

It follows that $\Phi_{4,cs}$ solves the RHP shown in Figure 18.

Remark 4.4. Note that $s = 0$ when $k_0 = 1$ or $x = -12t$ and we switch to the dispersive region. This switch is continuous in the sense that $s = 0 \Rightarrow a = b = 1$ and ϕ is the identity. The deformation automatically reduces to the deformation in the dispersive region. On the other side of the region, the curve defined by $8^{2/3} = -\log k_0^2/\tau$ lies to the right of the curve defined by $x = -(3t)^{1/3}\log(t)^{2/3}$. In the next section we address what happens as the curve defined by $8^{2/3} = -\log k_0^2/\tau$ is approached.

4.2.4 The Transition Region

While the collisionless shock region has extended the values of (x, t) for which there exists a well-behaved RHP past that of the dispersive region, it is not asymptotically reliable as we approach the Painlevé region: as $|x|$ decreases, a approaches the singularity of the parametrix at zero. To avoid this issue, we collapse the
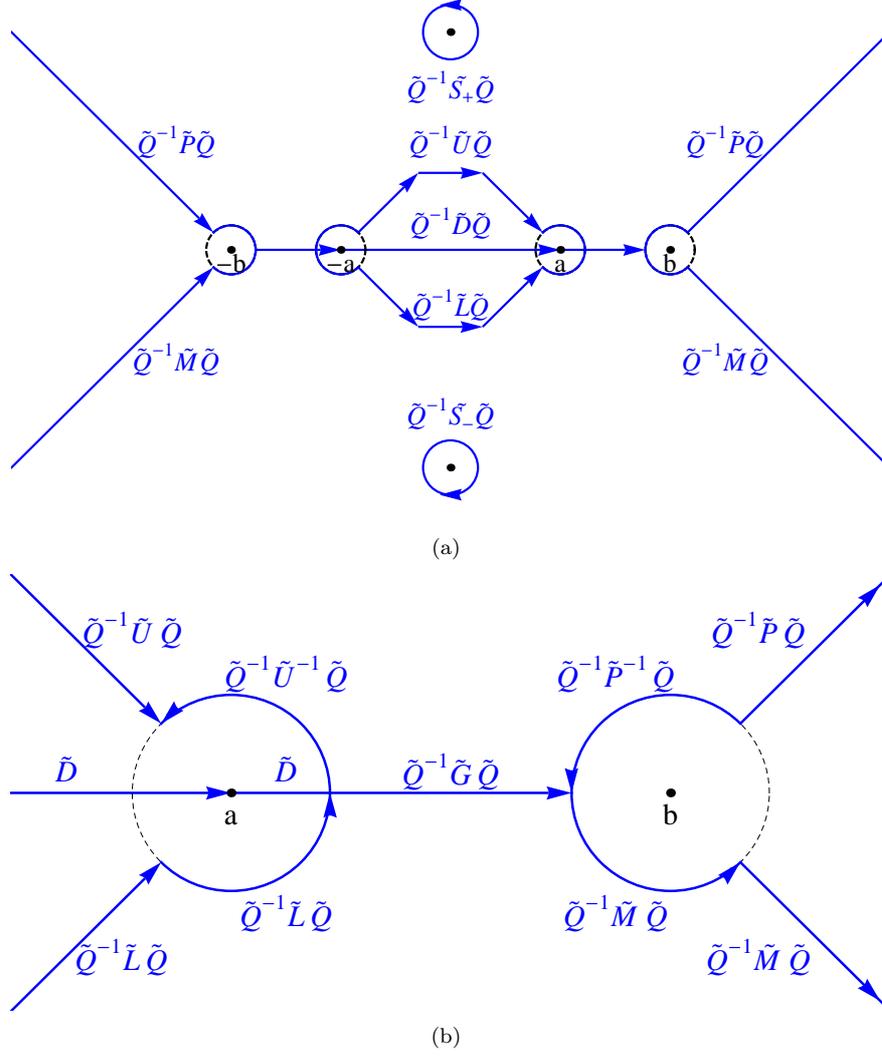
Figure 16: (a) The initial deformation of the RHP in the collisionless shock region for a function $\Phi_{1,cs}$. (b) The initial jump contours and matrices near a, b.

lensing. To maintain numerical accuracy, we choose a to ensure that the oscillations are controlled on $[-b, b]$. For simplicity let $x = -t^{1/3} R(t)$, where

$$\lim_{t \to \infty} \frac{R(t)}{\log(t)^{2/3}} = 0, \text{ and } \lim_{t \to \infty} R(t) = \infty.$$

Given a positive bounded function $f(x, t)$, we choose a so that

$$i\tau(g^+(k) + g^-(k)) = if(x, t), \quad k \in [a, b], \tag{4.3}$$

which implies

$$i\tau(g^+(k) + g^-(k)) = -if(x, t), \quad k \in [-b, -a].$$

In light of (C.3) this is equivalent to solving

$$f(x, t)/\tau = 24 \int_0^a \sqrt{(a^2 - p^2)(b^2 - p^2)} dp, \tag{4.4}$$

26
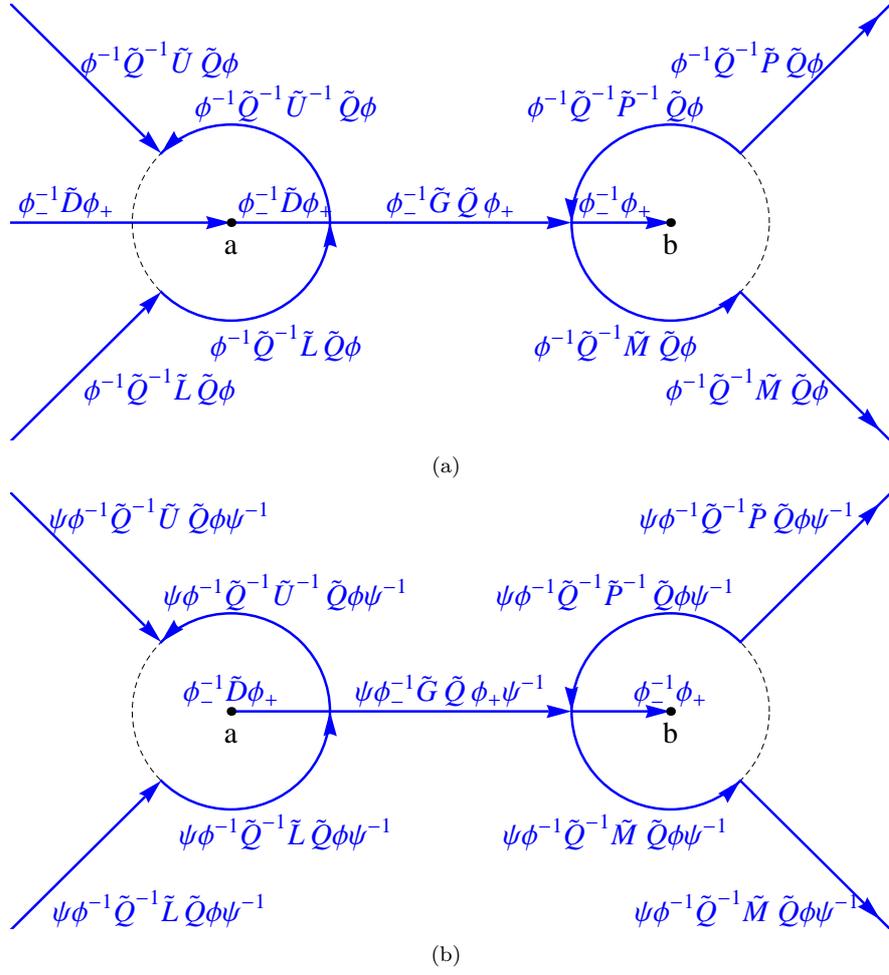
Figure 17: (a) The jump contours and matrices for the RHP for $\Phi_{2,cs}$ near a, b, (b) The jump contours and matrices for the RHP for $\Phi_{3,cs}$ near a, b.

for a and b. By adjusting f this can be solved since the right-hand side is a monotone function of a, under the constraint $a^2 + b^2 = 2$, which increases from 0 to 16 as a increases from 0 to 1. Furthermore, $\tau \to \infty$ in this region.

The RHP, after conjugation by ϕ, is of the form (4.2) and we claim that all entries of the matrices in (4.2) are bounded and the oscillations are controlled. In choosing (4.3) we have that $|i\tau(g^+(k) + g^-(k))| \leq f(x, t)$ on $[-b, b]$ which implies that the $(1, 2)$ and $(2, 1)$ components of the matrix have controlled oscillations and are bounded. Next, consider $i\tau(g^+(k) - g^-(k))$. The choice (4.3) implies

$$h(x,t)/\tau = 24 \int_a^b \sqrt{(p^2 - a^2)(b^2 - p^2)}dp, \qquad (4.5)$$

for a positive function h such that $1/C < h(x,t)/\tau + f(x,t)/\tau < C$, $C > 1$. This comes from the fact that both (4.5) and (4.4) cannot vanish simultaneously. Since f is chosen to be bounded, $h = \mathcal{O}(\tau)$ and $\tau = \mathcal{O}(R^{3/2}(t))$. Using these facts along with $k_0^2 = \mathcal{O}(R(t)/t^{2/3})$ we obtain

$$\lim_{t \to \infty} e^{-h(x,t)} = 0, \quad \lim_{t \to \infty} k_0^2 e^{h(x,t)} \to 0.$$

This shows that the $(1, 1)$ and $(2, 2)$ components of the matrices in (4.2) are bounded. These matrices are stable asymptotically for numerics without any lensing on $[-b, b]$. After lensing on $(-\infty, -b) \cup (b, \infty)$ we
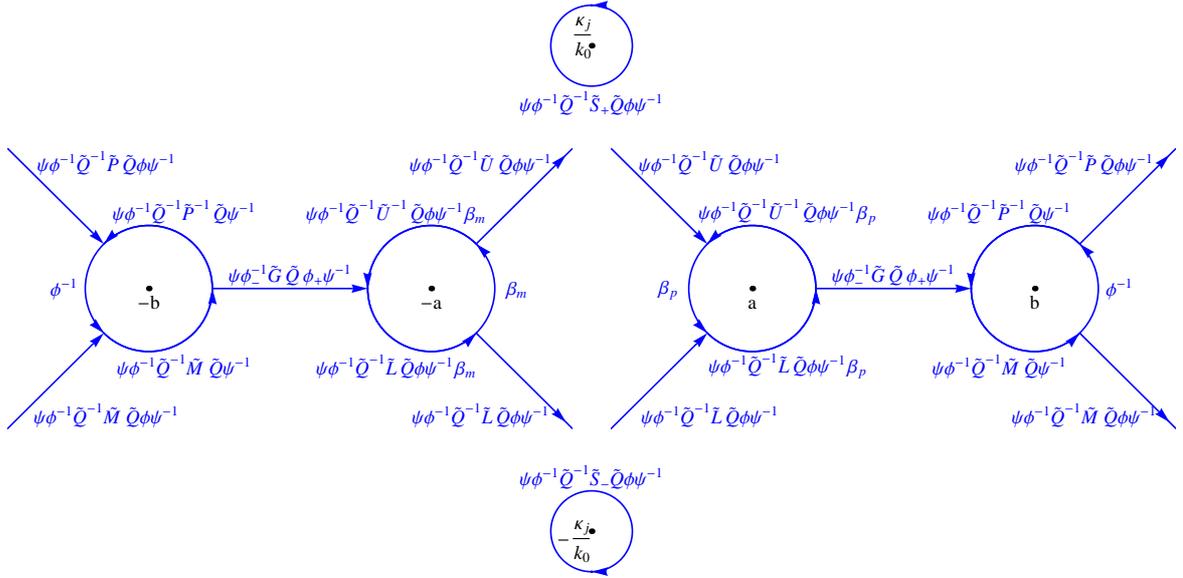
Figure 18: A zoomed view of the jump contours and matrices of the final deformation of the RHP in the collisionless shock region.

obtain a RHP for $\Phi_{1,t}$, see Figure 19(a). Define $\Phi_{2,t} = \Phi_{1,t}\phi$ and refer to Figure 20 for the jump contours and jump matrices of the RHP for $\Phi_{2,t}$ near a, b. Finally, define

$$\Phi_{3,t} = \begin{cases} \Phi_{2,t}\phi^{-1} & \text{inside the circles centered at } \pm b, \pm a, \\ \Phi_{2,t} & \text{otherwise.} \end{cases}$$

Refer to Figure 21 for the jump contours and jump matrices of the final RHP in the transition region.

4.2.5 Soliton Region

This is the region where $x > 0, x = \mathcal{O}(t)$. We present a deformation that is very similar to that used for mKdV. We use the $G = MP$ factorization, and the only complication arises from dealing with the jumps on $A_j^{\pm}$. As $|k_0|$ increases, the line $\text{Im}\,k = \sqrt{3}|k_0|$ eventually overtakes the circles, corresponding to solitons, or to the poles in the RHP. This means that we need to invert the exponentials on some of these circles but not on others. We illustrate this process. Define

$$Q_{k_0} = \begin{pmatrix} \prod_{|\kappa_j| < \sqrt{3}|k_0|}(k + \kappa_j)/(k - \kappa_j) & 0 \\ 0 & \prod_{|\kappa_j| < \sqrt{3}|k_0|}(k - \kappa_j)/(k + \kappa_j) \end{pmatrix}.$$

This matrix allows us to change the matrix $T_{\pm}$ to $S_{\pm}$ as we did in §4.2.1 for just those of the $A_j^{\pm}$ such that $|\kappa_j| < \sqrt{3}|k_0|$. Again we use a function $0 \leq \alpha(x,t) < \sqrt{3}|k_0|$. The reader is referred to Figure 22 for the final deformation.

4.3 Numerical Results

As in §3.3 we scale and truncate the contours appropriately and $q(n, x, t)$ is defined to be the solution obtained with n collocation points on each contour.
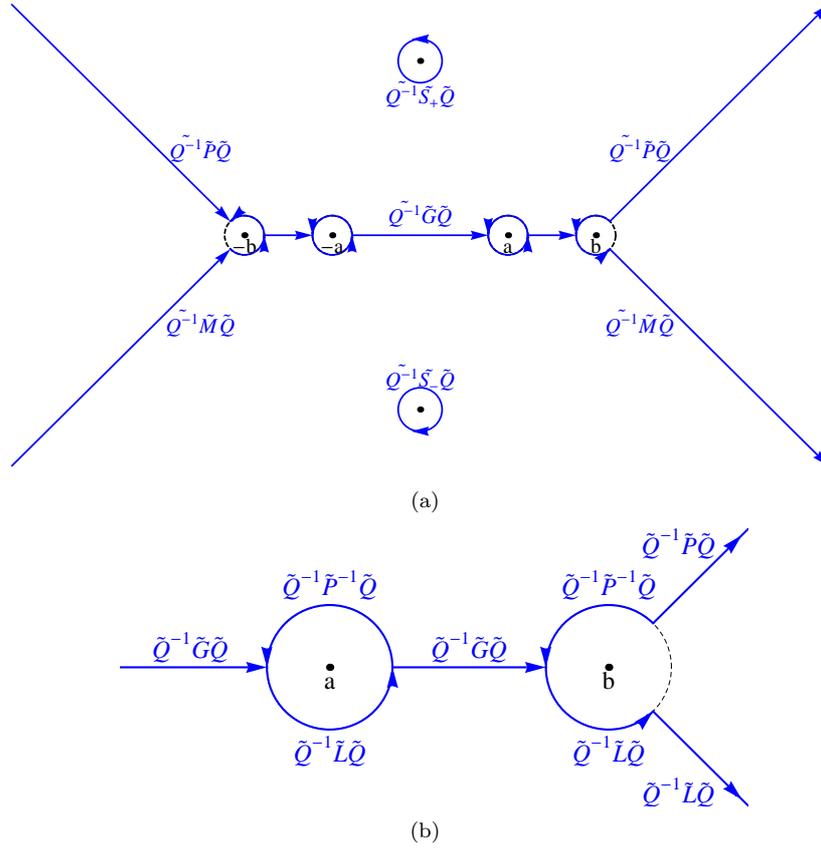
(a)

(b)

Figure 19: (a) The jump contours and matrices of the RHP for $\Phi_{1,t}$. (b) The jump contours and matrices of the RHP for $\Phi_{1,t}$ near a, b.

4.3.1 Direct Scattering

As a test case to verify the computed reflection coefficient we use an exact form given in [4]. If $q(x, 0) = A \operatorname{sech}^2(x)$ then

$$\rho(k) = \frac{a(k)\Gamma(\tilde{c}(k))\Gamma(\tilde{c}(k) - \tilde{a}(k) - \tilde{b}(k))}{\Gamma(\tilde{c}(k) - \tilde{a}(k))\Gamma(\tilde{c}(k) - \tilde{b}(k))}, \quad a(k) = \frac{\Gamma(\tilde{a}(k))\Gamma(\tilde{b}(k))}{\Gamma(\tilde{c}(k))\Gamma(\tilde{a}(k) + \tilde{b}(k) - \tilde{c}(k))},$$
$$\tilde{a}(k) = 1/2 - ik + (A + 1/4)^{1/2}, \quad \tilde{b}(k) = 1/2 - ik - (A + 1/4)^{1/2}, \quad \tilde{c}(k) = 1 - ik,$$

where Γ is the Gamma function. If $A > 0$ the set of poles is not empty. The poles are given by

$$\kappa_j = i((A + 1/4)^{1/2} - (j + 1/4)), \quad j = 1, \ldots \quad \text{while} \quad ((A + 1/4)^{1/2} - (j + 1/4)) > 0,$$

and the corresponding residues C_j are computed from the expression for ρ. Figure 23(a) shows the error between this relation and the computed reflection coefficient when $A = 2.4$ for a varying number of collocation points.

4.3.2 Inverse Scattering

As before, throughout this section we assume the reflection coefficient is obtained to machine precision.

1. *Convergence.* To analyze error we again use

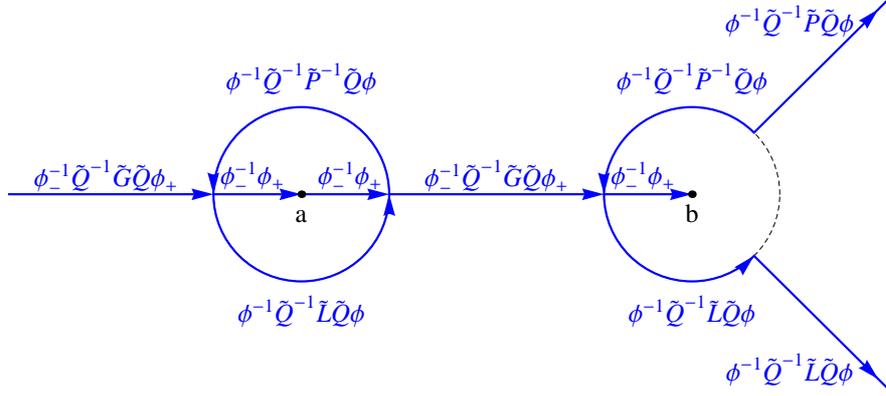$$Q_n^m(x, t) = |q(n, x, t) - q(m, x, t)|.$$

29

Figure 20: The jump contours and matrices of the RHP for $\Phi_{2,t}$ near a, b.
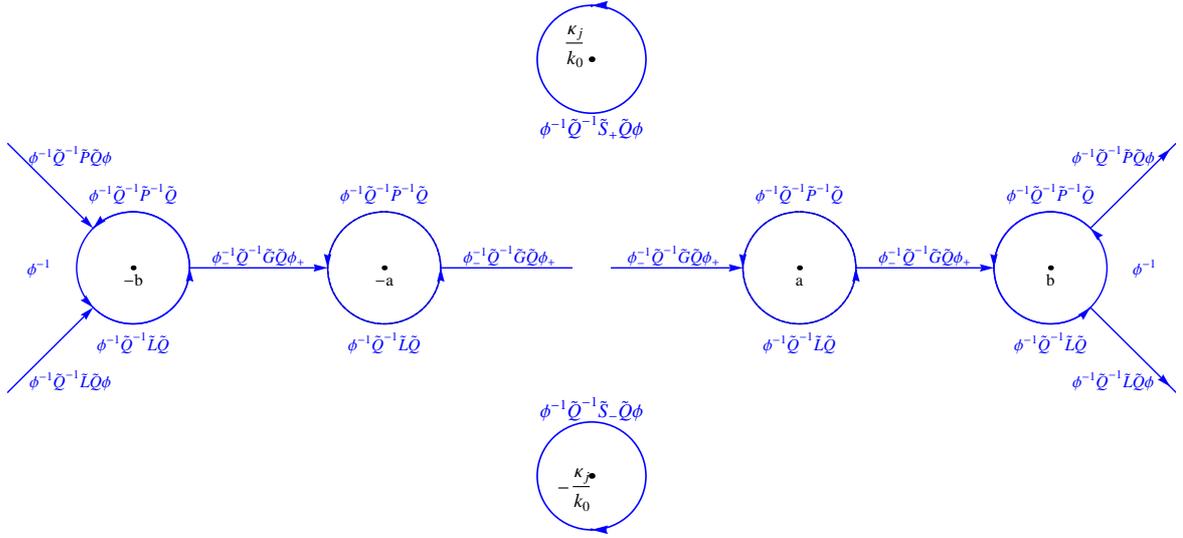

Figure 21: A zoomed view of the jump contours and matrices of the final deformation of the RHP in the transition region.

See Figure 24 for a demonstration of spectral convergence with all deformations.

2. *Asymptotic Stability.* As mentioned before, for the method to be stable we need that for a given n and m, $Q_n^m(x, t)$ should remain bounded (and small) as $|x| + |t|$ becomes large. Again, what we numerically demonstrate is that $Q_n^m(x, t)$ tends to zero in all regions. See Figure 25 for the demonstration of this.

4.3.3 Comparison with Asymptotic Formulae

In this section we compare our numerics with the asymptotic formulae for KdV. We skip the soliton region because the numerics limit to the linear system related to the soliton solutions exponentially fast. We also skip the transition region because, as mentioned before, no asymptotic results are known. As before, we emphasize that in view of the verified convergence, the numerical results are presumed to be more accurate than the asymptotic results.

1. *The Dispersive Region.* Numerical results are compared with the asymptotic formula (2.17) in Figure 26. The difference between the numerical approximation and the asymptotic approximation is of the correct order.
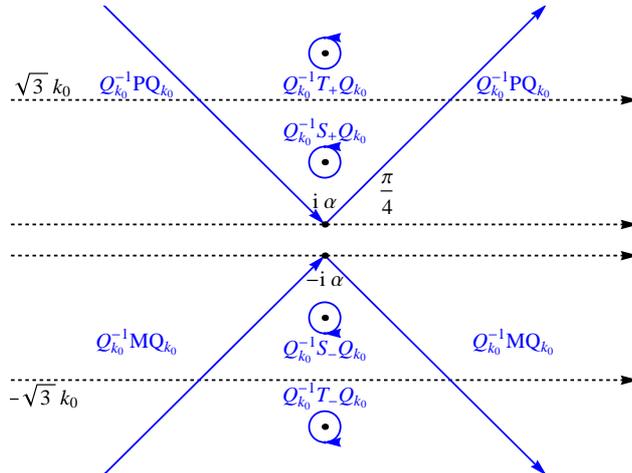
Figure 22: The final deformation of the RHP in the soliton region for KdV. The solution to this problem contains two solitons to illustrate when $T_\pm$ needs to be replaced with $S_\pm$.

2. *The Painlevé Region.* Numerical results are compared with the asymptotic formula in (2.15) in Figure 26. As before, we use the Riemann–Hilbert based techniques in [24] to compute v.

3. *The Collisionless Shock Region.* Numerical results are compared with the W from (2.16) in Figure 27. From Figure 27(b) we estimate the amplitude of the solution to be on the order of $|x|/t$. This allows us to estimate relative error, Figure 27(c). We see the relative error is on the order of $(\log t)^{-2/3}$ along the trajectory $x = 4(3t)^{1/3}(\log t)^{2/3}$. Numerically, in absolute error

$$q(x,t) - W(x,t) = \mathcal{O}\left(\frac{|x|}{t}(\log t)^{-2/3} \right).$$

Since there is not an error bound present in [7] we conjecture

$$q(x,t) - W(x,t) = \mathcal{O}(t^{-2/3}) \text{ as } t \to \infty, \quad x = C(3t)^{1/3}(\log t)^{2/3}, \quad C > 0.$$

Remark 4.5. In the collisionless shock region we compute the asymptotic expression by directly solving the limiting RHP numerically, instead of using the formula given in [7]. In our numerical experiments, this formula did not agree with Figure 27(a). This discrepancy will be explored further in a future paper.

4.4 Miura Transformation

Assume q satisfies the defocusing version of mKdV (1.2) then $u = -q^2 - q_x$ satisfies KdV (1.1). This is the well-known Miura transformation [25]. The numerical approach used here allows for q_x to be computed in a straightforward way, by essentially differentiating the linear system [24]. In Figure 28 we use the Miura transformation to check the consistency of our numerics for $q(x,0) = -1.3\,\mathrm{sech}^2(x)$. As expected, the evolution of KdV and the Miura transformation of mKdV coincide.

5 Summary

Through the synthesis of numerical methods with the method of inverse scattering we obtain an efficient numerical method for the solution of integrable PDEs. Furthermore, we make no physical domain approximations and fully capture dispersion. This ability to capture dispersion allows one to use our numerical method as a benchmarking tool for future numerical methods designed to capture dispersion. Using steepest descent to motivate the deformations of the RHPs we retain accuracy in asymptotic regimes. Our numerical method
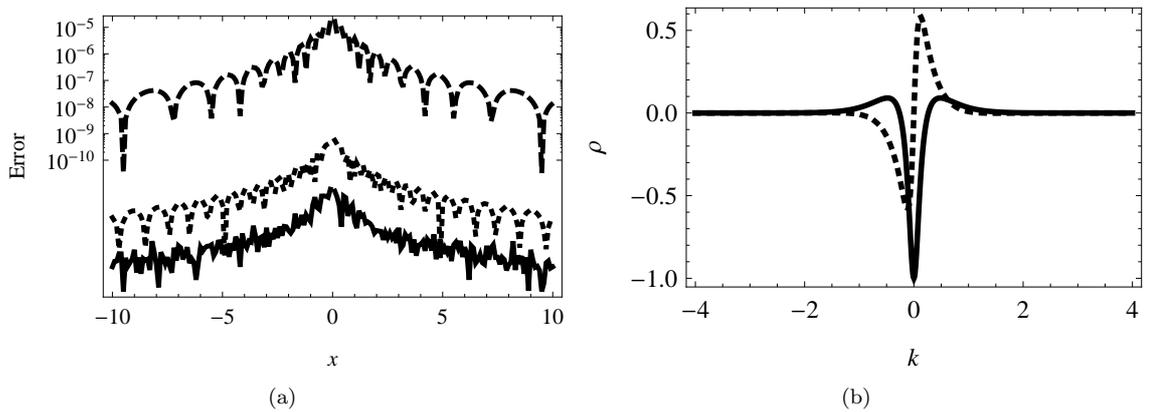
Figure 23: Numerical computation of the reflection coefficient $\rho(k)$ with $q(x,0) = 2.4\,\mathrm{sech}^2(x)$. (a) Absolute error between computed and actual reflection coefficient plotted vs. k when the number of collocation points is 25 (dotted), 50 (dashed) and 100 (solid), (b) Plot of the computed reflection coefficient with 100 collocation points. The real part is shown as a curve and the imaginary part as a dashed graph.

can aid in the derivation of asymptotic formulae and provide checks for error estimates. This method can be readily applied to other integrable equations on the whole line such as the focusing modified Korteweg-de Vries equation and the focusing and defocusing nonlinear Schrödinger equations. These successes also point to the method being useful for integrable PDEs on the half line and finite intervals using the Fokas method [26].

Acknowledgments

A Lensing

Here we go over, in detail, the process of lensing a RHP. To our knowledge, there is not an explicit tutorial describing this present in the literature. We start with a RHP (Figure 29(b))

$$\Phi_1^+(k) = \Phi_1^-(k)G(k), \quad k \in \Gamma \subset \mathbb{R},$$
$$\Phi_1(\infty) = I.$$

We choose $\Gamma \subset \mathbb{R}$ for simplicity and assume $0 \in \Gamma$. Assume that G has a factorization

$$G(k) = M_3(k)M_2(k)M_1(k),$$

such that all matrices have unit determinant. Fix an $r > 0$ and define the regions Ω_i, $i = 1, 2, 3, 4$, see Figure 29(a), by

$$\Omega_1 = \{k \in \mathbb{C} : \mathrm{Im}\,k > 0 \text{ and } |k| > r\},$$
$$\Omega_2 = \{k \in \mathbb{C} : \mathrm{Im}\,k < 0 \text{ and } |k| > r\},$$
$$\Omega_3 = \{k \in \mathbb{C} : \mathrm{Im}\,k > 0 \text{ and } |k| < r\},$$
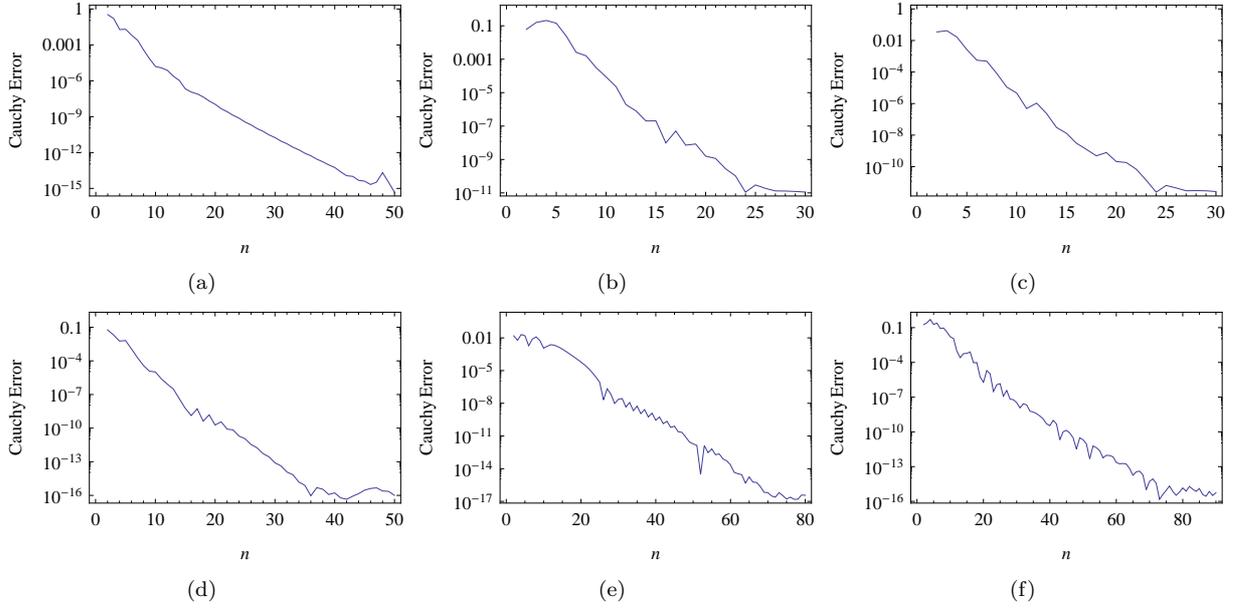$$\Omega_4 = \{k \in \mathbb{C} : \mathrm{Im}\,k > 0 \text{ and } |k| < r\}.$$

32

Figure 24: Demonstration of spectral convergence for KdV with $q(x,0)$ shown in Figure 2(a). All plots have $Q_{2m}^n(x,t)$ plotted as a function of n as n ranges from 2 to m. (a) *The Dispersive Region*: $m = 50$ at the point $(x,t) = (-10, 1/2)$, (b) *The Collisionless Shock Region*: $m = 30$ at the point $(-9.86, 2.8)$, (c) *The Transition Region*: $m = 30$ at the point $(-3.12, 7.)$, (d) *The Painlevé Region*: $m = 50$ at the point $(-2.76, 7)$, (e) *The Painlevé Region*: $m = 80$ at the point $(2.76, 7)$, (f) *The Soliton Region*: $m = 90$ at the point $(1.2, .1)$.

Further assume that M_3 has an analytic extension in a neighborhood of Ω_4 and M_1 has an analytic extension in a neighborhood of Ω_3. We wish (for whatever reason) to change the RHP on $(-r, r)$ by a lensing process. Define a new function Φ_2 by (Figure 29(c))

$$\Phi_2(k) = \begin{cases} \Phi_1(k)M_1^{-1}(k), & \text{if } k \in \Omega_3, \\ \Phi_1(k)M_3(k), & \text{if } k \in \Omega_4, \\ \Phi_1(k), & \text{otherwise.} \end{cases}$$

Define new contours Γ_i, $i = 1, 2, 3, 4, 5$, all oriented in the direction of increasing real part, by

$$\begin{aligned} \Gamma_1 &= \Gamma \cap (-\infty, r), \\ \Gamma_2 &= \{k \in \mathbb{C} : \operatorname{Im} k > 0 \text{ and } |k| = r\}, \\ \Gamma_3 &= (-r, r), \\ \Gamma_4 &= \{k \in \mathbb{C} : \operatorname{Im} k < 0 \text{ and } |k| - r\}, \\ \Gamma_5 &= \Gamma \cap (r, \infty). \end{aligned}$$

We can compute the jumps of Φ_2 on these contours. As an example consider Γ_2. Set

$$\Phi_2^+(k) = \Phi_2^-(k)U(k), \quad k \in \Gamma_2,$$

for some matrix $U(k)$ to be determined. In this case $\Phi_2^+(k) = \Phi_1^+(k) = \Phi_1^-(k) = \Phi_2^-(k)M_1(k)$. We find that $U(k) = M_1(k)$. Repeating this process on all contours show that Φ_2 satisfies the following RHP (Figure
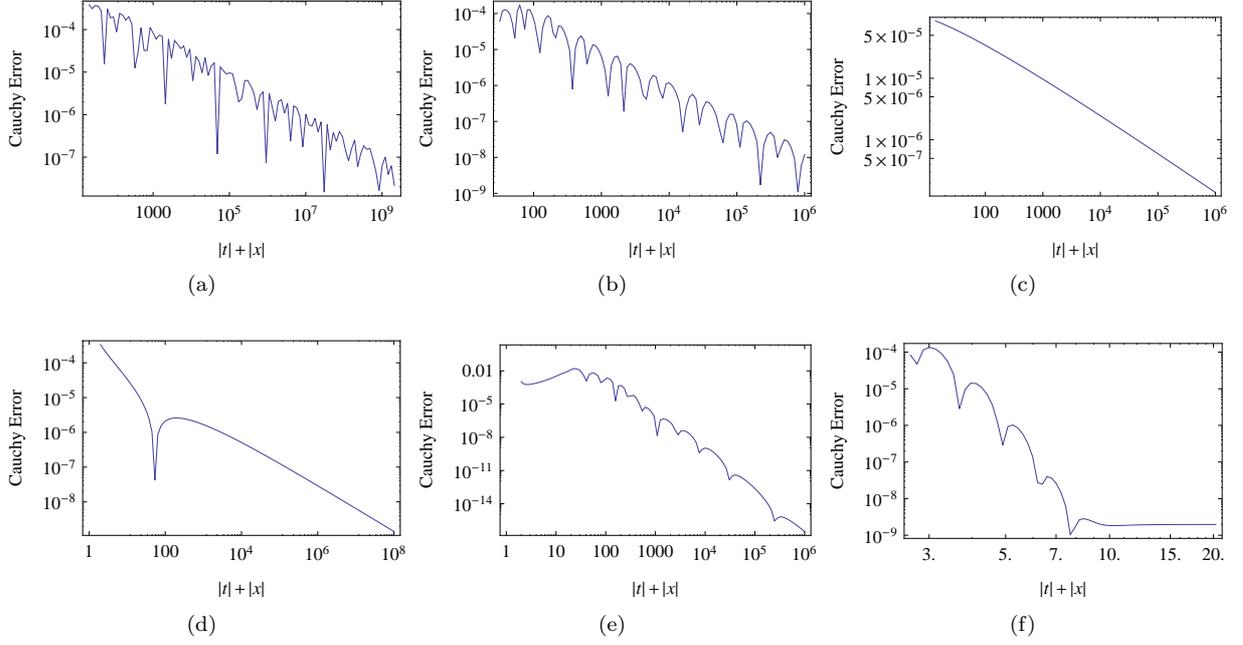
Figure 25: Demonstration of asymptotic stability for KdV with $q(x,0)$ shown in Figure 2(a). All plots have $Q_m^n(x,t)$ plotted as a function of $|x| + |t|$. (a) *The Dispersive Region*: $m = 16$, $n = 8$ along the trajectory $x = -20t$, (b) *The Collisionless Shock Region*: $m = 20$, $n = 20$ along the trajectory $x = -4(3t)^{1/3} \log(t)^{2/3}$. (c) *The Transition Region*: $m = 16$, $n = 8$ along the trajectory $x = -(3t)^{1/3} \log(t)^{1/6}$, (d) *The Painlevé Region*: $m = 16$, $n = 8$ along the trajectory $x = -t^{1/3}$, (e) *The Painlevé Region*: $m = 32$, $n = 16$ along the trajectory $x = t^{1/3}$, (f) *The Soliton Region*: $m = 32$, $n = 16$ along the trajectory $x = 4t - 2.3$, in order to track the soliton.

29(d))

$$
\Phi_2^+(k) = \begin{cases} \Phi_2^-(k) G(k), & \text{if } k \in \Gamma_1, \\ \Phi_2^-(k) M_1(k), & \text{if } k \in \Gamma_2, \\ \Phi_2^-(k) M_2(k), & \text{if } k \in \Gamma_3, \\ \Phi_2^-(k) M_3(k), & \text{if } k \in \Gamma_4, \\ \Phi_2^-(k) G(k), & \text{if } k \in \Gamma_5, \end{cases}
$$

$$
\Phi_2(\infty) = I.
$$

It is clear that this generalizes to contours off the line and is only limited by the analyticity properties of the factorization. Furthermore, if $M_1, M_3 \to I$ as $k \to \infty$ in the proper regions the lensing can be employed in infinite regions. Note that one of the matrices M_i could be the identity in which case we drop that contour from the RHP.

B   Diagonal Riemann–Hilbert Problems

We consider RHPs of the form

$$
\Phi^+(k) = \Phi^-(k) D(k), \quad k \in \Gamma, \quad \Phi(\infty) = I, \quad \Phi : \mathbb{C} \to C^{n \times n}, \tag{B.1}
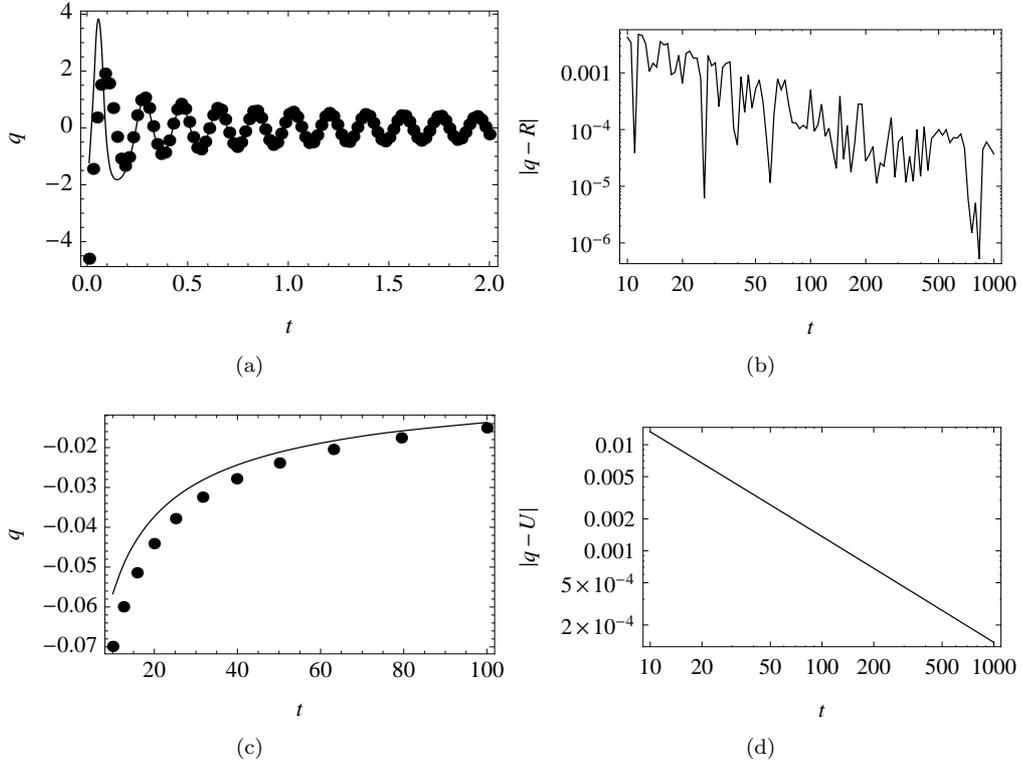$$

Figure 26: Numerical asymptotics in the dispersive and Painlevé regions for KdV. (a) *The Dispersive Region:* $q(10, x, t)$ and $R(x, t)$ plotted as a function of t with $x = -20t$. $R(x, t)$ is defined in (2.17). Solid: Computed solution, Dots: Asymptotic formula, (b) *The Dispersive Region:* $|q(10, x, t) - R(x, t)|$ plotted as function of t with $x = -20t$. A least-squares fit gives $|q(10, x, t) - R(x, t)| = \mathcal{O}(t^{-1.1})$, (c) *The Painlevé Region:* $q(10, x, t)$ and $U(x, t)$ plotted as a function of t with $x = -t^{1/3}$. $U(x, t)$ is defined in (2.15). Solid: Computed solution, Dots: Asymptotic formula, (d) *The Painlevé Region:* $|q(10, x, t) - U(x, t)|$ plotted as a function of t with $x = -t^{1/3}$. A least-squares fit gives $|q(10, x, t) - U(x, t)| = \mathcal{O}(t^{-0.99})$ which is in agreement with the error bound.
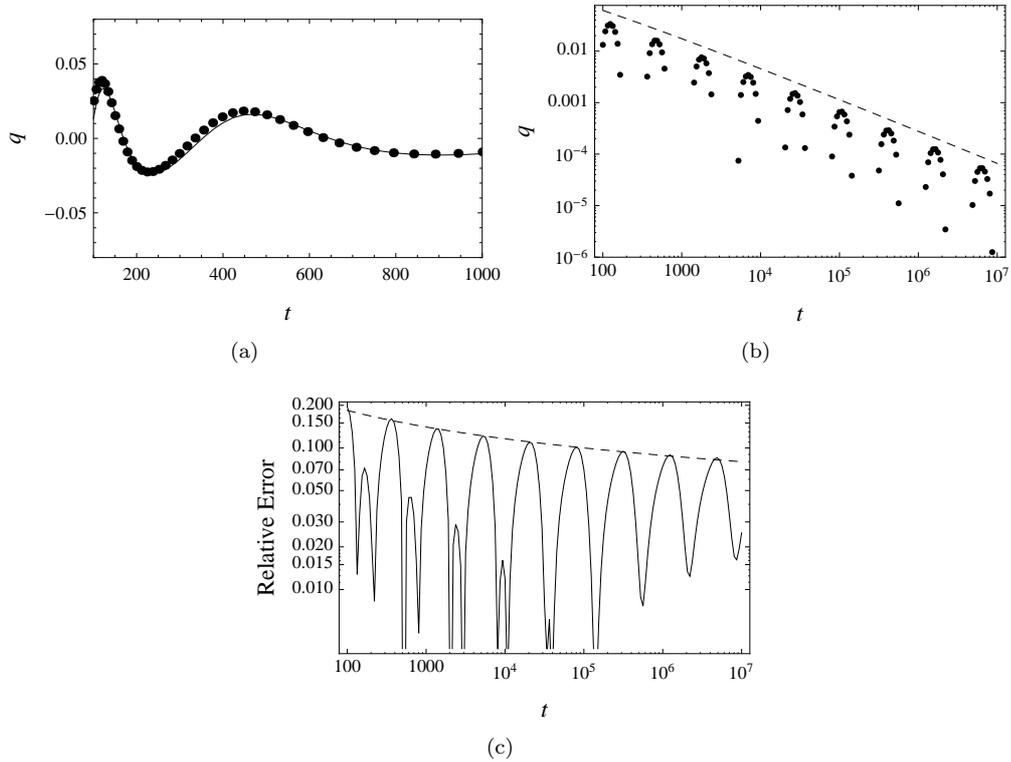
(a)

(b)

(c)

Figure 27: Numerical asymptotics in the collisionless shock region for KdV. (a) $q(10, x, t)$ and $W(x, t)$ plotted as a function or t with $x = 4(3t)^{1/3}(\log t)^{2/3}$. Solid: Computed solution, Dots: Computed solution to (2.16), (b) Confirmation that the amplitude is on the order of $|x|/t$ along the same trajectory. Dots: Computed solution, Dashed: $t \mapsto -x/(12t)$, (c) Confirmation that the relative error is on the order of $(\log t)^{-2/3}$. Solid: $t \mapsto |q(10, x, t) - W(x, t)|/(|x|/t)$, Dashed: $t \mapsto (\log t)^{-2/3}$, along the same trajectory.
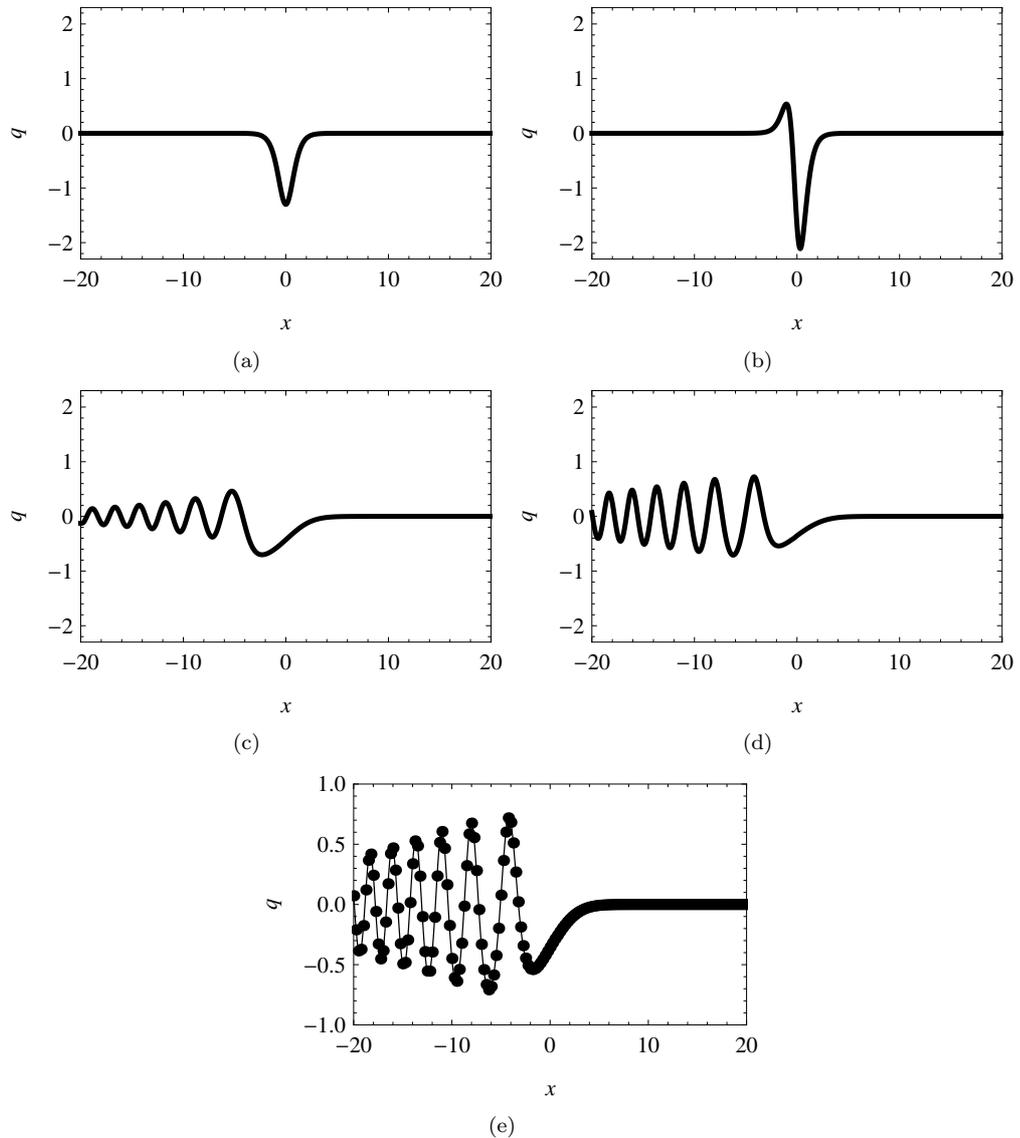
Figure 28: Numerical demonstration of the consistency of the numerical methods for KdV and mKdV through the Miura transformation. (a) Initial condition for mKdV, $q(x,0) = q_0(x) = -1.3\,\mathrm{sech}^2(x)$, (b) Initial condition for KdV, $q(x,0) = -q_0^2(x) - \frac{d}{dx}q_0(x)$, (c) Evolution using mKdV at $t = .75$, (d) Evolution using KdV at $t = .75$, (e) Solid: Evolution using KdV at $t = .75$, Dots: Miura transformation of the evolution using mKdV at $t = .75$.
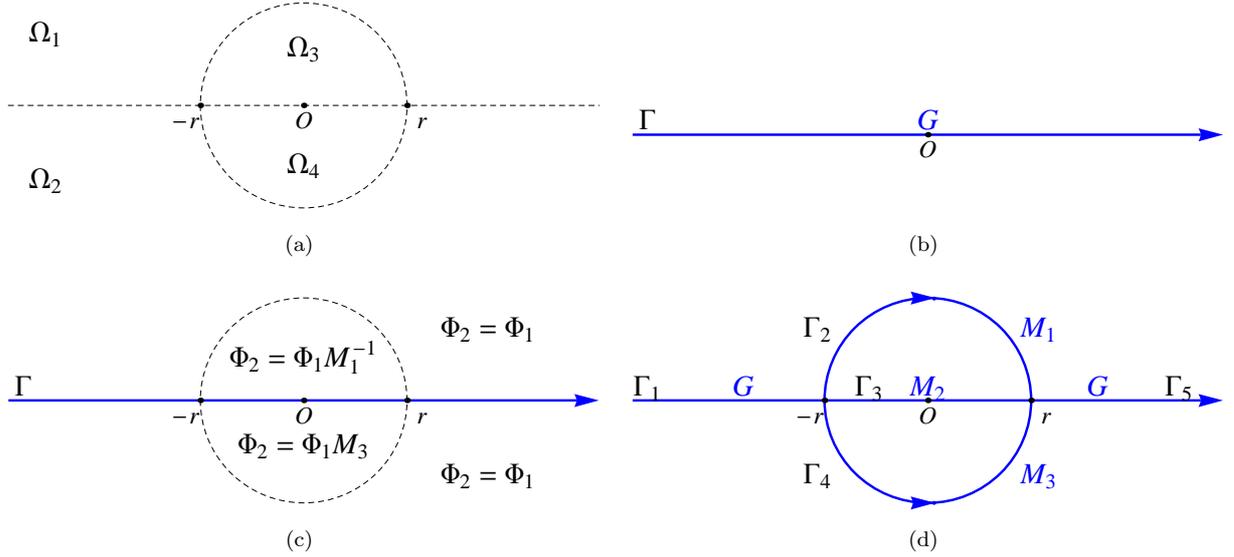
Figure 29: The lensing process. (a) Regions in the complex k-plane, (b) Contours and jump matrices for the RHP for Φ_1, (c) Definition of Φ_2, (d) Contours and jump matrices for the RHP for Φ_2.

and $D(k) = \mathrm{diag}(d_1(k), \ldots, d_{nn}(k))$ with $\det D(k) = 1$. For the most general case, we assume that $\log d_i(k) \in L^2(\Gamma)$ for each i and the $\pm$ limits are taken in the L^2 sense [10]. We decouple (B.1) into n scalar RHPs:

$$\phi_i^+(k) = \phi_i^-(k) d_i(k), \quad k \in \Gamma, \quad \phi_i(\infty) = 1, \quad i = 1, \ldots, n. \tag{B.2}$$

Each of these has a solution

$$\phi_i(k) = \exp\left(\frac{1}{2\pi i} \int_\Gamma \frac{\log d_i(s)}{s - k} ds\right) \exp\left(\mathcal{C}_\Gamma \log d_i(k)\right).$$

We compute the Cauchy transform using the techniques of [16], which is accurate and reliable throughout the complex plane. A solution of (B.1) is given by $\Phi(k) = \mathrm{diag}(\phi_1(k), \ldots, \phi_n(k))$. Under the assumption that $\det D(k) = 1$, the solution is unique [11].

Consider the RHP (3.2)

$$\Delta^+(k) = \Delta^-(k) \begin{pmatrix} 1 - \rho(-k)\rho(k) & 0 \\ 0 & 1/(1 - \rho(-k)\rho(k)) \end{pmatrix}, \quad k \in (-k_0, k_0), \quad \Delta(\infty) = I.$$

The unique solution is given by

$$\Delta(k) = \begin{pmatrix} \delta(k) & 0 \\ 0 & \delta^{-1}(k) \end{pmatrix}, \quad \delta(k) = \exp\left(\frac{1}{2\pi i} \int_{-k_0}^{k_0} \frac{\log(1 - \rho(-s)\rho(s))}{s - k} ds\right).$$

C g-function

We give the explicit form of g from §4.2.3. Restricting to $a^2 + b^2 = 2$, the expression

$$s = 24 \int_a^b \sqrt{(p^2 - a^2)(b^2 - p^2)} dp, \quad \tau = tk_0^3, \quad s = -\log k_0^2/\tau \in [0, 8^{2/3}],$$

defines both $a(s)$ and $b(s)$ since it is a monotone function of a. Define the g-function to be

$$g(k) = 12 \int_{b(s)}^k \sqrt{(p^2 - a^2(s))(p^2 - b^2(s))} dp + 12 \int_0^{a(s)} \sqrt{(p^2 - a^2(s))(p^2 - b^2(s))} dp, \tag{C.1}$$

we choose the branch cuts for $\sqrt{(p^2 - a^2(s))(p^2 - b^2(s))}$ to be the straight line segments along $[-b(s), -a(s)]$ and $[a(s), b(s)]$. In order for g to be single-valued it is necessary to add a branch cut on $[-a(s), a(s)]$.

Lemma C.1. The g-function given by (C.1) satisfies:

1. g is bounded in the finite plane,

2.
$$
g^+(k) - g^-(k) = \begin{cases} 24 \int_{b(s)}^{k} \sqrt{(p^2 - a^2(s))(p^2 - b^2(s))}dp, & \text{if } k \in [a(s), b(s)], \\ 24 \int_{b(s)}^{a(s)} \sqrt{(p^2 - a^2(s))(p^2 - b^2(s))}dp, & \text{if } k \in (-a(s), a(s)), \\ 24 \int_{-b(s)}^{k} \sqrt{(p^2 - a^2(s))(p^2 - b^2(s))}dp, & \text{if } k \in [-b(s), -a(s)], \\ 0, & \text{otherwise,} \end{cases} \tag{C.2}
$$

3.
$$
g^+(k) + g^-(k) = \begin{cases} 24 \int_{0}^{a(s)} \sqrt{(p^2 - a^2(s))(p^2 - b^2(s))}dp, & \text{if } k \in [a(s), b(s)], \\ 24 \int_{0}^{k} \sqrt{(p^2 - a^2(s))(p^2 - b^2(s))}dp, & \text{if } k \in (-a(s), a(s)), \\ 24 \int_{0}^{-a(s)} \sqrt{(p^2 - a^2(s))(p^2 - b^2(s))}dp, & \text{if } k \in [-b(s), -a(s)], \\ 2g(k), & \text{otherwise,} \end{cases} \tag{C.3}
$$

4.
$$
g(k) = 4k^3 - 12k + \mathcal{O}(k^{-1}) \text{ as } k \to \infty,
$$

5.
$$
k_0^2 e^{i\tau(g^+(k) + g^-(k))} = 1, \text{ for } k \in (-a(s), a(s)).
$$

Proof. (1) is clear from (C.1). (2) and (3) follow from contour integration and the fact that the integrand is invariant under $p \mapsto -p$. To prove (4) we look at the expansion of the integrand
$$
12\sqrt{(p^2 - a^2(s))(p^2 - b^2(s))} = 12p^2\sqrt{(1 - (a(s)/p)^2 - (b(s)/p)^2 - (a(s)/p)^2(b(s)/p)^2)}.
$$
We use
$$
\sqrt{1 - y} = 1 - \frac{1}{2}y - \frac{1}{8}y^2 + \dots,
$$
to obtain (for large p)
$$
12\sqrt{(p^2 - a^2(s))(p^2 - b^2(s))} = 12p^2(1 - (a(s)/p)^2 - (b(s)/p)^2) + \mathcal{O}(p^{-2}).
$$
After integrating this we find
$$
f(k) = \int_{a(s)}^{k} \sqrt{(p^2 - a^2(s))(p^2 - b^2(s))}dp = 4k^3 - 6(a^2(s) + b^2(s))k + C + \mathcal{O}(k^{-1}),
$$
for some complex constant C. To find C notice that $f(k)$ is the sum of a constant and odd powers of k,
$$
f(k) + f(-k) = 2C,
$$
$$
= \int_{a(s)}^{k} \sqrt{(p^2 - a^2(s))(p^2 - b^2(s))}dp + \int_{a(s)}^{-k} \sqrt{(p^2 - a^2(s))(p^2 - b^2(s))}dp
$$
$$
= \int_{a(s)}^{k} \sqrt{(p^2 - a^2(s))(p^2 - b^2(s))}dp + \int_{k}^{-a(s)} \sqrt{(p^2 - a^2(s))(p^2 - b^2(s))}dp
$$
$$
= -\int_{-a(s)}^{a(s)} \sqrt{(p^2 - a^2(s))(p^2 - b^2(s))}dp
$$
$$
= -2\int_{0}^{a(s)} \sqrt{(p^2 - a^2(s))(p^2 - b^2(s))}dp.
$$

39

Therefore $g(k) \backsim 4k^2 - 12k + \mathcal{O}(k^{-1})$, where we used $a^2(s) + b^2(s) = 2$. Finally, for (5) assume $k \in (-a(s), a(s))$,

$$-\log k_0^2/\tau = 24 \int_{a(s)}^{b(s)} \sqrt{(p^2 - a^2(s))(b^2(s) - p^2)} dp,$$

$$\log k_0^2/\tau = 24i \int_{a(s)}^{b(s)} \sqrt{(p^2 - a^2(s))(p^2 - b^2(s))} dp = i(g^+(k) - g^-(k)),$$

$$k_0^2 e^{i\tau(g^+(k) - g^-(k))} = 1.$$

■

These are all the properties mentioned in §4.2.3.

References

[1] K. Atkinson and W. Han. *Theoretical Numerical Analysis.* Springer, New York, NY, 2009.

[2] D.J. Korteweg and G. de Vries. On the change of form of long waves advancing in a rectangular canal, and on a new type of long stationary waves. *Philosophical Magazine*, 39:422–443, 1895.

[3] C. S. Gardner, J. M. Greene, M. D Kruskal, and R. M. Miura. Method for solving the Korteweg–de Vries equation. *Phys. Rev. Lett.*, 19:1095–1097, 1967.

[4] P. G. Drazin and R. S. Johnson. *Solitons: an introduction.* Cambridge University Press, New York, NY, 1996.

[5] S. Olver. A general framework for solving Riemann-Hilbert problems numerically. *Submitted for publication*, 2010.

[6] P. Deift and X. Zhou. A steepest descent method for oscillatory Riemann-Hilbert problems. Asymptotics for the MKdV equation. *Annals of Mathematics*, 137(2):295–368, 1993.

[7] P. Deift, X. Zhou, and S. Venakides. The collisionless shock region for the long-time behavior of solutions of the KdV equation. *Comm. Pure and Appl. Math.*, 47:199–206, 1994.

[8] K. Grunert and G. Teschl. Long-time asymptotics for the Korteweg–de Vries equation via nonlinear steepest descent. *Math. Phys., Anal. and Geom.*, 12:287–324, 2008.

[9] M. J. Ablowitz and A. S. Fokas. *Complex Variables: Introduction and Applications.* Cambridge University Press, New York, NY, 2005.

[10] P. Deift. *Orthogonal Polynomials and Random Matricies: A Riemann-Hilbert Approach.* New York University Press, New York, NY, 1999.

[11] X. Zhou. Riemann-Hilbert problems and integrable systems. *Lectures at MSRI*, 1999.

[12] K. Clancey and I. Gohberg. *Factorization of Matrix Functions and Singular Integral Operators.* Birkhauser Verlag, Boston, MA, 1981.

[13] M. Ablowitz and H. Segur. *Solitons and the Inverse Scattering Transform.* SIAM, Philadelpha, PA, 1981.

[14] M. J. Ablowitz and P. A. Clarkson. *Solitons, Nonlinear Evolution Equations and Inverse Scattering.* Cambridge University Press, New York, NY, 1991.

[15] R. Beals and R. R. Coifman. Scattering and inverse scattering for first order systems. *Comm. Pure Appl. Math.*, 37:39–90, 1984.

[16] S. Olver. Computing the hilbert transform and its inverse. *Math. Comp*, 80:1745–1767, 2011.

[17] S. P. Hastings and J. B. McLeod. A boundary-value problem associated with the second Painlevé transcendent and the Korteweg–de Vries equation. *Arch. Rational Mech. Anal*, 73:31–51, 1980.

[18] H. Segur and M. Ablowitz. Asymptotic solutions of nonlinear equations and a Painlevé transcendent. *Physica D*, 1-2:165–184, 1981.

[19] B. Deconinck and J. N. Kutz. Computing spectra of linear operators using the Floquet-Fourier-Hill method. *Journal of Comp. Phys.*, 291(1):296–321, 2007.

[20] Y. Saad and M.H. Schultz. GMRES: A generalized minimal residual algorithm for solving nonsymmetric linear systems. *SIAM J. Sci. Stat. Comput.*, 7(3):856–869, 1986.

[21] S. Olver. GMRES for the differentiation operator. *SIAM J. Numer. Anal.*, 114:607–628, 2009.

[22] P. Deift, X. Zhou, and S. Venakides. An extension of the steepest descent method for Riemann-Hilbert problems: the small dispersion limit of the Korteweg–de Vries equation. *Proc. Natl. Acad. Sci.*, 95(2):450–454, 1998.

[23] S. Olver. Computation of equilibrium measures. *J. Approx. Theory*, 163:1185–1207, 2011.

[24] S. Olver. Numerical solution of Riemann-Hilbert problems: Painlevé II. *Found. of Comp. Math.*, 11:153–179, 2011.

[25] R. M. Miura. Korteweg–de Vries equation and generalizations. I. a remarkable nonlinear transformation. *J. Math. Phys.*, 9:1202–1204, 1968.

[26] A. S. Fokas. *A Unified Approach to Boundary Value Problems*. SIAM, Philadelphia, PA, 2008.